



## In This Issue

*Charles  
Stelzried  
and  
Michael  
Klein*

### Technology—Communication Systems

Abhijit Biswas, in “Overview of Optical Communications,” provides a tour of an optical deep space communication system with key elements or subsystems. NASA needs additional communications capacity to maintain a virtual presence throughout the solar system. Optical frequency deep space communication systems are expected to provide wider signal bandwidths as compared with current microwave frequencies. In addition, optical systems with their shorter operating wavelengths compared to microwave will have smaller and lighter-weight spacecraft components.

Aluizio Prata, et al., in “Compact High-Efficiency Displaced-Axis Axially

Symmetric High-Gain Antenna for Spacecraft Communications,” show the advantages for spacecraft communications of the compact high-gain antenna design achieved with the axially displaced ellipse (ADE) concept. A comparison between the Cassegrain and ADE antennas indicates the advantages of the ADE design. The ADE design has been chosen for the high-gain antenna communications to Earth of the Mars Reconnaissance Orbiter (MRO), scheduled for launch in 2005.

### Technology—Information Systems

Anastassios Petropoulos’ contribution, “Low-Thrust Spiralling Trajectory Design,” stresses the importance of the highly efficient use of propellant devices with low-thrust propulsion. Ion propulsion systems, for example, can have ten times or greater the efficiency of chemical rockets, but current methods of trajectory design fall short of being able to effectively leverage this improved efficiency. The article describes the design of low-thrust trajectories for escape, capture, and orbit transfers around planetary bodies.

Jay Gao, in “Simulation Tools for Protocol Design and Evaluation,” states that a communication protocol can provide multiple data transfer services as well as cost-saving automation. A simulation-based approach is useful for verifying the behavior of the communication protocols and quantifying the potential benefit of new protocol designs for future NASA missions. The simulation environment is described along with examples that show the substantial level of fidelity afforded by these simulations.

## C O N T E N T S

### Technology

Overview of Optical Communications.....	3
Compact High-Efficiency Displaced-Axis Axially Symmetric High-Gain Antenna for Spacecraft Communications .....	9
Low-Thrust Spiralling Trajectory Design.....	15
Simulation Tools for Protocol Design and Evaluation .....	18
Space-Based Middleware Technology .....	24
UAV-to-Ground Optical Communications Transceiver .....	31
The Large Millimeter Telescope .....	36

### Science

MASERs, Black Holes, and the Age of the Universe .....	40
--	----

Norman Lamarra, in “Space-Based Middleware Technology,” views middleware as “any software involved in connecting separate application pieces (components).” He discusses middleware evolution, a component approach, standardization, reduced costs, and a middleware-enabled space web. Space-based middleware is expected to provide increased capability for automation and space assets cooperation.

#### **Technology—Non-Deep Space**

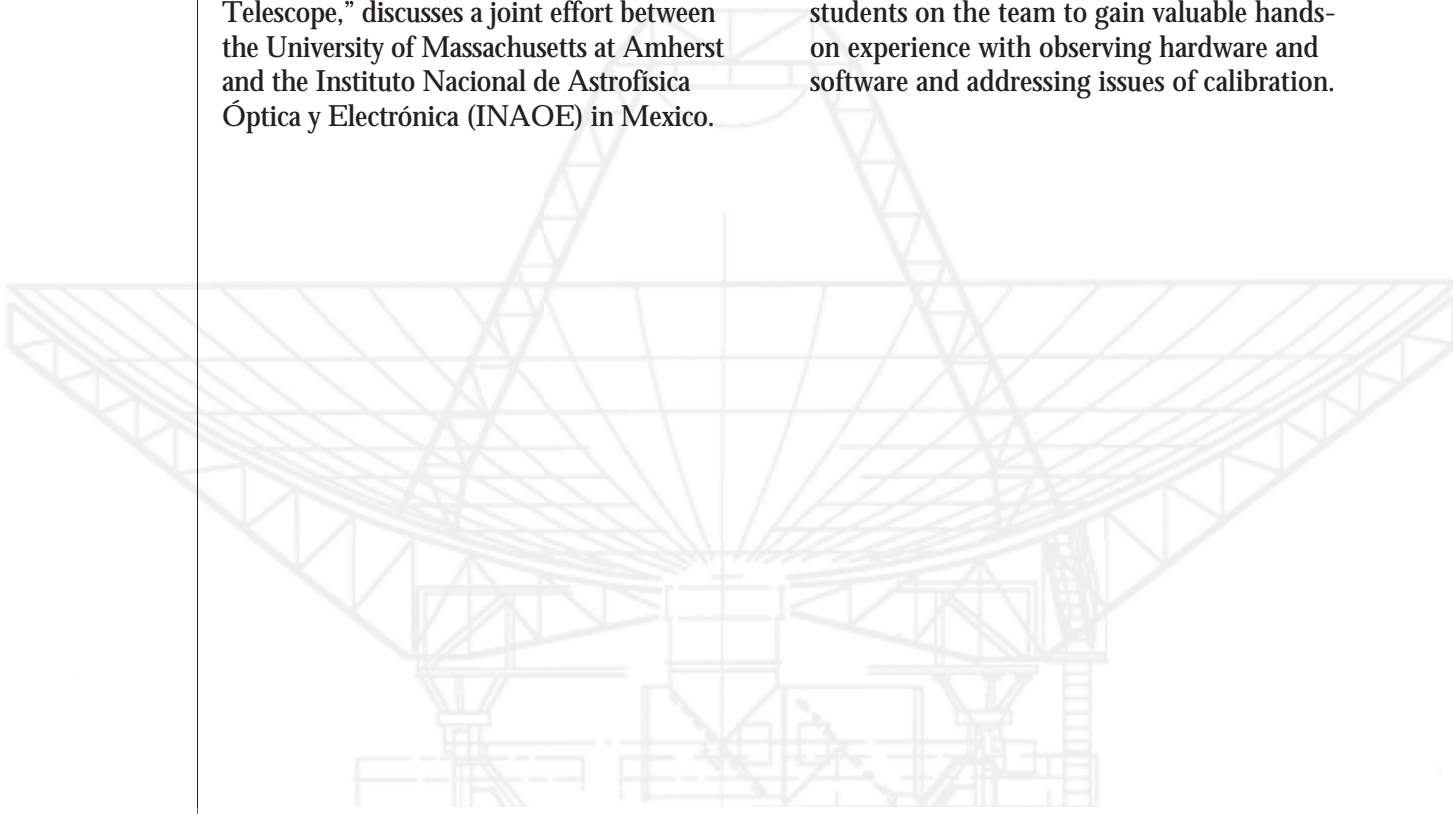
Abhijit Biswas and Keith Wilson, in “UAV-to-Ground Optical Communications Transceiver,” describe the demonstration of optical communications to ground for an unmanned aerial vehicle (UAV). The communications consist of both high-rate downlink and uplink between an airborne UAV and a ground station. This demonstration is expected to result in UAVs equipped with optical communications systems smaller and lighter than existing microwave systems, with much improved capabilities, achieving data rates of 2–10 gigabits per second (Gbps). The optical communications terminal (OCT) design for this demonstration is described.

Alfonso Feria, in “The Large Millimeter Telescope,” discusses a joint effort between the University of Massachusetts at Amherst and the Instituto Nacional de Astrofísica Óptica y Electrónica (INAOE) in Mexico.

They are constructing a 50-meter (m)-diameter Large Millimeter Telescope (LMT) to operate between 100 and 300 gigahertz (GHz) at the Sierra Negra site 4,600 m above sea level. The goal is to make the highest-sensitivity measurements ever achieved at these frequencies, allowing data to be collected from the first visible structures of the universe. Engineering support is supplied by JPL.

#### **Science**

Tom Kuiper of JPL and Lincoln Greenhill of the Smithsonian Astrophysical Observatory (SAO) team up to describe how their DSN radio astronomy observations of 22-GHz microwave amplification by stimulated emission of radiation (MASER) lines from water molecules reveal important characteristics of the supermassive black holes at the center of distant galaxies. Using a combination of spectroscopic and interferometric techniques, Greenhill’s radio astronomy team is accurately measuring the masses and distances to the black holes and deriving the shapes of their accretion disks. The authors of “MASERs, Black Holes, and the Size of the Universe” describe how the research and development environment of the DSN complexes enables the three graduate students on the team to gain valuable hands-on experience with observing hardware and software and addressing issues of calibration.





# Overview of Optical Communications

## Introduction

NASA requires expanded communications capacity over interplanetary distances in order to enable the use of high resolution science instruments and maintain a virtual presence throughout the solar system. The bandwidth explosion afforded by utilizing optical frequencies for interplanetary communications will very likely play a critical role in satisfying this objective. The benefits of optical technology are by no means limited to deep space. In fact, near-Earth satellite communications are on the threshold of revolutionizing achievable data rates in the wake of successful optical flight demonstrations in the US [1] and Europe [2]. This article, however, is limited to providing an overview of the technology elements relevant to deep space optical communications.

Based upon link analysis and the current state of technology data rates of at least 10 megabits per second (Mbps) from the farthest range to Mars are viable. This would require approximately 35–50 kilograms (kg) mass and 100–150 watts (W) of prime spacecraft power. As a point of reference, the combined X/Ka-band system being considered for the Mars Reconnaissance Orbiter (MRO) will transmit at 0.6 Mbps from maximum Mars range, weighs 65 kg and will utilize 200 W of power. Therefore, optical technology nominally holds the promise of a 14–18-decibel (dB) improvement in terms of bits/kg/W. Of course, realizing the potential benefits will require some brisk technology validation, as well as development. In the remainder of this article some of the issues will be briefly discussed.

Figure 1 provides a schematic overview of an optical communications system that shows the key elements or subsystems involved.

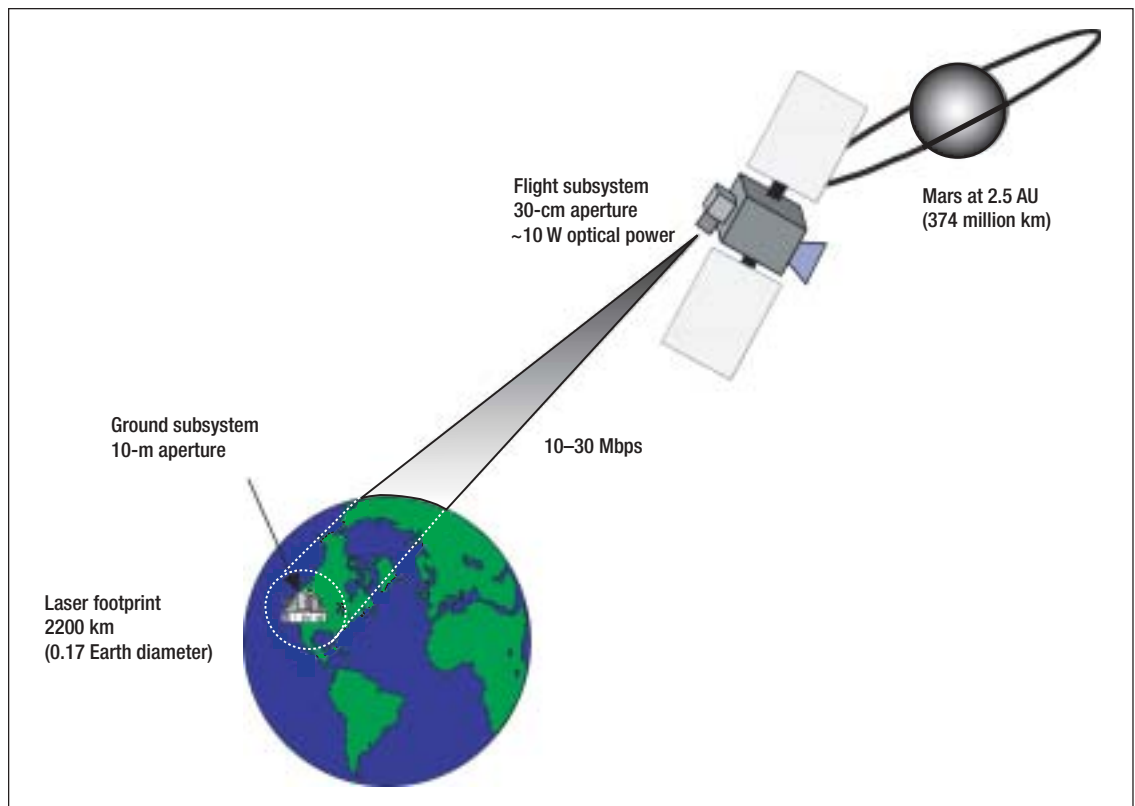
## Channel Considerations

The physical channel encountered in establishing an optical link from a planetary probe to Earth depends, to a large extent, upon receiving antennas performance and location. A sufficient number of photons must be detected in order to enable information extraction at the desired high data rates. Therefore, large-area (equivalent to 10-meter (m)-diameter) photon collectors are required. Receiving antennas on the ground must be configured as a globally distributed network, taking advantage of weather diversity in order to overcome line-of-sight blockage due to clouds, as well as accounting for the obscuration caused by the rotation of the Earth. Previous studies have determined that 7–9 globally distributed antennas can achieve the desired coverage and availability.

Propagation of the laser beam transmitted from deep space through the Earth's atmosphere is an important channel consideration for ground-based antennas. First, signal attenuation due to absorption and scattering of laser light by atmospheric constituents occurs. Second, random refractive index fluctuations of the atmosphere cause perturbations of the otherwise nearly plane laser beam wave front. The nature of the perturbation is such that when the laser light is collected and focused by an otherwise nearly perfect optical system, the focal spot is enlarged relative to what it would have been in the absence of the atmosphere. Stated differently, the field of view for detecting laser light propagating through the atmosphere is increased. The increase or spot-size enlargement factor is related to the extent of refractive index fluctuations or the severity of "atmospheric turbulence."

*Abhijit Biswas*

Figure 1. Elements of an optical communications system for a link from Mars at 2.5 AU utilizing a ground-based receiver. With a 10% wall-plug efficiency, 100 W of electrical power is required for the laser with approximately 10 W of optical output.



Ground-based receiving antennas are also subjected to background photon noise contributed by sky radiance, or scattering of sunlight by atmospheric constituents. While optical filtering can reject a bulk of the out-of-band background light, a fraction coincident with the laser wavelength contributes to detected background photon noise. The focal spot enlargement due to atmospheric turbulence, mentioned above, also implies a larger field of view and consequently a proportional increase in detected background noise. Thus, daytime optical links when the atmospheric turbulence tends to be more severe will also involve a larger contribution from background noise due to Earth's sky radiance. This problem becomes particularly formidable when the Sun-Earth probe (SEP) angles are small. Vulnerability to stray light that falls upon the detector from outside the field of view can also become a critical issue at low SEP angles when the receiving antenna must look past the Sun. The effect of the background is an effective degradation of the signal-to-noise ratio and hence reduced data rate.

Atmospheric degradation of the optical

link can be mitigated through site selection. For example, locating receiving stations 2-3 km above sea level will significantly reduce both sky radiance and atmospheric turbulence. A second and more powerful mitigation strategy is to use active approaches that allow reconstruction of the plane wave front, thereby reducing the field of view [3], as well as adaptive algorithms to selectively reject background noise through use of array detectors [4].

Channel effects related to the Earth's atmosphere and cloud blockage could largely be overcome by deploying large receiving antennas above the Earth's atmosphere. Indeed, orbiting receivers have long been viewed as an attractive option. The resulting reduction in background noise will also relax to some extent the aperture size required to achieve equivalent performance as ground receivers. Nevertheless, 5-7-m diameter apertures will be required. The cost of deploying orbiting optical communication receivers, however, is extremely high. Vulnerability to the potential risk of a single point of failure also cannot be overlooked. For the cost of a single orbiting receiver, a

complete ground network can be developed and operated. Therefore, while awaiting technology advancement that will devise cost-effective and practical deployment of large aperture orbiting receivers, a ground network that will provide the experience and optimization of optical receivers seems a compelling choice. Balloons and/or other airborne assets that can serve as stable platforms for large-area optical receivers are also emerging as a new option. These platforms will place the receivers above clouds, at altitudes that will result in negligible atmospheric turbulence and sky radiance. Payload capacity, station keeping, and strategies for acquiring and tracking the spacecraft laser signal need to be thoroughly investigated.

All of the optical receivers discussed above will be subject to sunlight reflected from planets as well as stars that happen to fall within the detector field of view. While optical filtering can significantly reduce noise, complete elimination cannot be achieved. The optical filtering used must also take into account Doppler line-shifts of the laser wavelengths that are being transmitted from deep space. Either the filters must be broad enough to accommodate the line-shifts or they must be actively tunable.

## Flight Subsystem

### *Optical Communications Terminal*

Optical communications utilize transceivers capable of simultaneous transmission and reception of light through a common aperture. Additionally, sensors and steering devices are integrated into the optomechanical assembly in order to enable closed-loop pointing control of the transmitted laser beam. Figure 2 shows a 30-centimeter (cm)-diameter silicon carbide (SiC) telescope developed by industry as a prototype optical communications transceiver. The telescope body and mirrors are made of the same material so that thermal expansion mismatches are eliminated. The telescope displayed uniform optical performance over a wide temperature range ( $-40^{\circ}\text{C}$  to  $50^{\circ}\text{C}$ ). Future deep space optical communications transceivers will rely on similar lightweight, stiff, and thermally stable optical telescopes.

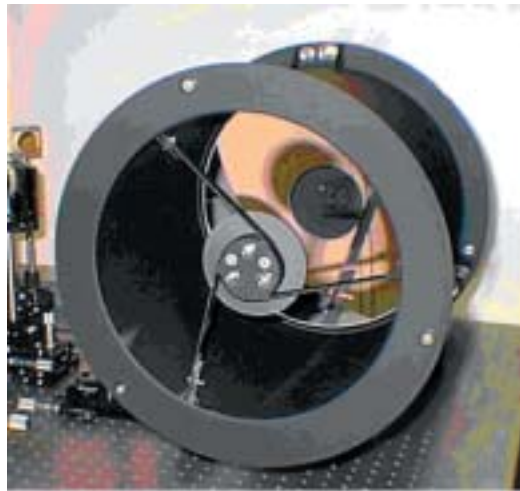


Figure 2.  
An example of a 30-cm-diameter all silicon carbide optical communications terminal developed by the Science Software Group (SSG, Inc.).

### *Acquisition Tracking and Pointing Strategies*

Foremost among the technical challenges in accomplishing deep space optical communications is pointing control of a narrow laser beam (see Figure 1) in the presence of disturbances due to spacecraft vibrations and attitude variations. To first order the beam divergence is the ratio of the transmitted wavelength to the aperture diameter. Thus the angular width (full-width at half maximum) of a 1-micrometer ( $\mu\text{m}$ )-wavelength laser transmitted through a 30-cm-diameter terminal is approximately 3.5 microrad ( $\mu\text{rad}$ ). The pointing control required is within approximately 10% of the beam width, and this includes aggregate static and dynamic mispointing errors. For reference, this is nearly two orders of magnitude tighter than typical microwave telecommunications antenna pointing requirements (1–2-millirad (mrad)) but less than the 40-nanoradians pointing accuracy implemented in the Hubble Space Telescope (HST). While the gap with HST is somewhat reassuring, optical communications pointing control requires higher bandwidth.

The key element in implementing successful pointing strategies from deep space is a pointing reference that can be used for closed-loop control. Laser beacons broadcast from Earth stations and celestial sources such as planets and stars can all serve as optical pointing references.

Laser beacons that are broadcast from Earth with adequate signal delivered to the

spacecraft are excellent pointing references. Clearly delivering adequate signal to the farthest reaches of the solar system will be required for the transmission of high-power lasers. Lasers transmitted to planetary probes from the Earth's surface suffer losses not only from atmospheric perturbations but also from spatial spreading of the beam. On the other hand, the complexity of deploying laser systems in high-altitude airborne or spaceborne platforms can be formidable and may not always be as cost effective as expending additional power on the ground. Ground lasers can also be made to approach near-diffraction widths by using active techniques that compensate for the atmospheric distortions. This can be achieved by utilizing adaptive optics techniques.

Given the potential complications in broadcasting lasers from Earth, celestial beacon sources are very attractive. Using celestial sources, such as stars, will usually involve weaker signals, requiring longer integration times and reducing the control bandwidths. Incidentally, this is also true for laser beacons at very long ranges. Therefore, the use of additional inertial sensors for interpolating between less frequent beacon updates is a strategy being pursued. Using sunlight scattered from planets, such as the Earth image as seen from planetary distances, is also viable though it is plagued by albedo and phase-angle variations that require smart algorithms to accurately extract pointing information. Recent studies have shown that Earth imaged at infrared wavelengths may afford a promising solution.

#### ***Laser Transmitter Technology***

Direct detection of intensity-modulated lasers is currently baselined for transmitting information back to Earth over deep space links. Though phase modulation followed by coherent detection can be advantageous, especially because of the insensitivity to background noise, practical considerations related to random phase fluctuations of the laser beam traversing Earth's atmosphere, coupled with the challenges of flying a frequency-stabilized laser, favor the direct detection approach. The high energy per pulse sought for deep space

communications, as elaborated below, favors the 1- $\mu\text{m}$ -wavelength region for deep space communications.

The average optical power emitted by the laser transmitter is constrained by prime power available on the spacecraft. Therefore, in order to overcome the range-dominated losses, the laser operates with a variable duty cycle (pulse repetition rate) so that higher energy pulses are emitted at lower duty cycles, thereby trading channel capacity for channel efficiency while ensuring that adequate photons per pulse are detected by the Earth receiver. Pulse position modulation (PPM) is used for transmitting multiple bits of information with a single laser pulse.

For laser pulse repetition frequencies of 100–400 kilohertz (kHz), diode-pumped, Q-switched, solid-state lasers are suitable. Developers are pursuing the packaging and qualification of these lasers, maintaining the highest possible wall-plug, or electrical-to-optical conversion efficiency. Such lasers were considered for the X2000 Europa mission study, for example. For shorter Mars ranges, higher-duty cycle lasers are needed in order to achieve 10–100-Mbps data rates. Advances in pulsed fiber amplifier lasers can satisfy the duty cycles suitable for these ranges. However, the peak powers achievable with these lasers are somewhat limited. Cavity-dumped, solid-state lasers are conceptually attractive, with relatively high duty cycles and peak-to-average laser powers. Laboratory breadboard-level development of cavity-dumped lasers is being pursued. All candidate laser transmitters for deep space suffer from rather low electrical-to-optical conversion efficiency, typically around 10%. This can in principle be improved to 20–30% without violating any fundamental physical principles; however, a focused development effort will be required since conventional laser applications provide no motivation to implement increased efficiency.

#### **Receiver Systems Technology**

A globally distributed network of large-aperture antennas is required to meet the requirements for an optical deep space network. The technology challenge is to

identify practical, cost-effective, relatively large-aperture (approximately 10-m-diameter) photon collectors. One approach is a segmented spherical light collector designed with adequate solar baffling and stray light rejection. This concept utilizes approximately 100 identical 1-m panels made of lightweight glass that are mounted on a single structure. Two-axis (tip-and-tilt) control of the individual panels is possible though not actively. Alignment control of the panels consists of ensuring that reflected light from each panel is directed to a common focal spot. The light collection scheme is tolerant to step displacement errors between the panels. So the segments behave like an array of 1-m mirrors that share a common structural mount. A dome along with baffling and perhaps an active contamination control system will allow the segmented panel array to provide daytime small SEP angle reception.

Recently, studies have been initiated to assess the suitability of an array of smaller-aperture telescopes that provide an effective collection diameter of several meters. For example, an architecture utilizing 100–250 telescopes, each with a 0.6- to 1-m diameter, is being studied as a receiving system [5]. Here the smaller individual apertures simplify the structural design, though efficient signal collection and processing will be required. Contamination control will also be more difficult for a large array of individual apertures than for a single, large-aperture antenna. Contamination control is important because otherwise stray light scattered from outside the field-of-view onto the detector can severely compromise the performance of the link.

Photon-starved links require efficient detection strategies. At the wavelength of interest (approximately 1  $\mu\text{m}$ ), high quantum efficiency photon counters are required. Near-infrared-enhanced Si, InGaAs or other III-V material-based photon-counting detectors are being considered in order to achieve the best quantum efficiency and sensitivity. High-bandwidth (0.5–1-gigahertz [GHz]) detectors with large collection areas are also required in addition to photon detection efficiency, because of the atmospheric blurring

of the focal spot discussed under channel considerations. These requirements are somewhat contradictory but can be achieved to first order at least in the lower-bandwidth regions. On the other hand, detector arrays are conceptually attractive devices that circumvent the large area problem and can potentially provide additional performance gains by the choice of adaptive algorithms whereby background noise can be selectively rejected. The development of both single, large-area, photon-counting devices and detector arrays is being pursued.

Additive electronics noise must be minimized during analog-conditioning by relying upon cooled electronics. Finally the detected and analog-conditioned electronic pulses are input into high-bandwidth digitizing circuits for processing. It is in the digital domain that synchronization algorithms are implemented. Frame, symbol, and slot synchronization must be accomplished on the incoming data stream followed by decoding. Reed-Solomon codes can perform reasonably well (~2.2 dB-gap from capacity) for higher-order pulse position modulation (PPM) signaling. Recently, new techniques based upon outer convolutional codes followed by an interleaver and accumulator, have been developed at JPL. These new codes offer near capacity (0.5- to 0.75-dB-gap) decoding for a wide range of PPM orders. Following encouraging results obtained with analysis and simulation, implementation of these decoders for laboratory testing is being initiated and should be accomplished in the next few years.

## Conclusion

A brief overview of the elements of free-space optical communications technology has been provided. Ongoing technology development is targeted towards a deep space flight demonstration in the next 6–7 years. Technology validation accomplished through flight experiments will accelerate the infusion of optical technology for NASA's expanded communications needs. The ability of a space-borne terminal to acquire and track an Earth receiving station

while pointing the narrow laser beam with submicroradian accuracy is perhaps one of the foremost issues that must be properly understood and verified. The electrical-to-optical efficiency of laser transmitters also needs improvement in order to render optical technology more power efficient. An Earth receiving infrastructure with assured high link availability should be carefully considered because without such an asset, the high data rates will not be realized. While the benefits of deploying such assets above clouds—or better still in, Earth orbit—are clear, the complexity and cost are formidable. An alternate, lower-risk precursor is a ground network that will provide operational experience and a better understanding and optimization of the optoelectronic receivers for deep space communications, while allowing lower-cost maintenance and upgrades.

Optical communications technology holds considerable promise for NASA's future deep space exploration missions. The use of high-resolution scientific probes that generate huge data volumes will become possible with the availability of this technology. Implementing these technologies will revolutionize the way of doing planetary science, with a virtual presence throughout the solar system becoming a reality.

## References

- [1] NRO and TRW (2001, May). The GeoLITE spacecraft. *Delta 2 Launch Report* [Online]. Available: <http://spaceflightnow.com/delta/d285/010517geolite.html>
- [2] T. Tolker-Nielsen and G. Oppenhauser, "In-orbit test results of an operational optical intersatellite link between ARTEMIS and SPOT4, SILEX," in *Free-Space Laser Communications Technologies XIV*, G. S. Mecherle, Ed. (*Proc. SPIE*, vol. 4635, 1, 2002).
- [3] K. Wilson, "Adaptive optics for high bandwidth deep space optical communications," JPL R&TD Strategic Initiative Proposal Award, 2003.
- [4] V. A. Vilnrotter and M. Srinivasan, "Adaptive detector arrays for optical communications receivers," *IEEE Transactions on Communications*, vol. 50, Issue 7, pp. 1091–1097, July 2002.
- [5] V. Vilnrotters and M. Srinivasan, "Optical array receiver for deep-space communication through atmospheric turbulence," JPL R&TD Small Proposal Award, 2003.



# Compact High-Efficiency Displaced-Axis Axially Symmetric High-Gain Antenna for Spacecraft Communications

## Introduction

As the technical sophistication of the instruments used in NASA's planetary missions increases, so does their demand on the communication channel data rates required to relay the acquired information back to Earth. Increased data rates require increased signal-to-noise ratios. Among the multitude of engineering parameters that can be used to improve the communication channel signal-to-noise ratio, increasing the antenna gain is an obvious choice. However, since the gain of any antenna is directly proportional to its collecting area, the current trend towards smaller spacecraft imposes a conflicting requirement that severely limits the maximum tolerable antenna aperture dimensions. The end result is an increasing need for aperture antennas that are simultaneously compact and efficient.

Since the early days of space exploration, most spacecraft high-gain antennas have employed axially symmetric, dual-reflector Cassegrain geometries [1]. Although not without problems, this ubiquitous configuration, derived from the classical Cassegrain telescope of optical fame, is robust, relatively simple, and capable of providing high gain and high efficiency as long as its reflectors are of sufficient size relative to the operational wavelength. In this article, another dual-reflector antenna configuration is discussed: the displaced-axis, dual-reflector antenna (usually referred to as the axially displaced ellipse, or ADE, antenna). This and other comparable antenna geometries have been studied by the authors

during the last five years [2]. It has been found that the ADE provides an excellent choice for compact high-gain spacecraft antenna applications. As the result of this study, which was partially supported by the Technology Program Office of the Interplanetary Network Directorate (IND), the ADE geometry was recently selected for use as the high-gain antenna of the Mars Reconnaissance Orbiter (MRO) spacecraft, currently scheduled for launch in 2005.

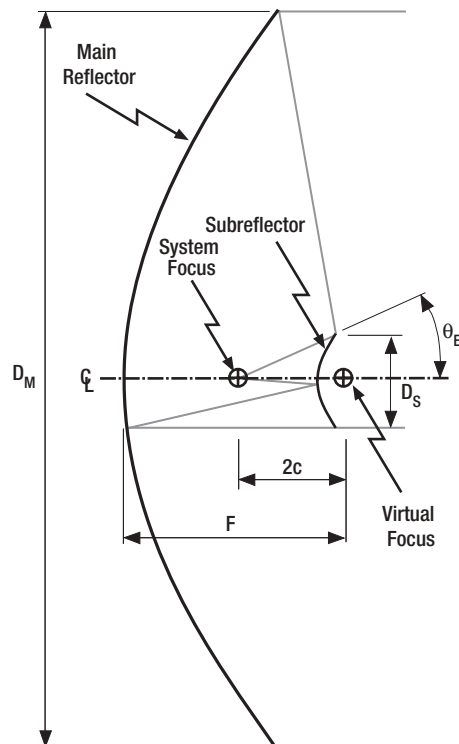
Several relevant electric aspects of the ADE configuration are discussed below. Since this antenna is presented here as an alternative to the typical Cassegrain geometry when a relatively small electric aperture size is needed, we start with an overview of the Cassegrain geometry and the corresponding difficulties that occur when its electric aperture is reduced. With this background, the ADE is introduced and its significant aspects are discussed. Whenever appropriate, the characteristics of the ADE and Cassegrain antennas are compared. To demonstrate the ADE antenna, as well as to validate the tools developed for its design and analysis, a prototype X-band ADE with an electrically small 1250-mm-diameter aperture (about 30 wavelengths at 7.145 GHz, which is considered a small diameter for dual-reflector antennas) was successfully constructed and measured as part of the Mars Surveyor 2001 program. This article concludes with a discussion of this early example of a compact ADE antenna, which although never used in space, is the precursor to the MRO spacecraft ADE antenna currently being made.

*Aluizio Prata, Jr.,  
Fernando J. S.  
Moreira, and  
Luis R. Amaro*

## The Ubiquitous Cassegrain and Some of Its Limitations

The classical Cassegrain configuration is shown in Figure 1. In order to provide a realistic example, this is a scale drawing of a compact practical geometry. This antenna employs an electrically large paraboloidal main reflector (diameter  $D_M$  and focal length  $F$ ) illuminated by a relatively smaller confocal coaxial hyperboloidal subreflector (diameter  $D_S$  and inter-focal distance  $2c$ ). In the transmit mode of operation a high-gain feed horn located at the system focus excites the subreflector, which in turn scatters the feed energy towards the main reflector (the main reflector is then illuminated from the virtual focus located behind the subreflector). Having the feed horn as near as possible to the main reflector vertex allows the associated communications electronics to be placed just behind the main reflector, minimizing the length, and hence the associated loss of the waveguide runs connecting the amplifiers to the feed horn. In this geometry the main reflector provides the desired gain, with the subreflector operating as a relay mirror that spreads the horn-radiated energy over the relatively large main reflector angular extension.

Figure 1.  
Classical  
Cassegrain  
antenna geometry.



The basic principle of operation of the Cassegrain, and almost any other reflector antennas, is geometrical optics (i.e., their operation assumes that the electromagnetic field can be described by rays). In this light, Figure 1 can be scaled up to any physical dimension, as long as all its relative proportions are preserved. However, to ensure proper operation when scaling down, the reflecting surfaces cannot become smaller than several wavelengths in extent—practical experience indicates that about 7 wavelengths is a reasonable lower limit for most geometries. If excessively small surfaces are used, the electric performance of the antenna proportionally degrades significantly. Also, since the subreflector is always substantially smaller than the main reflector, as the antenna electric dimensions are reduced, the subreflector will reach the above wavelength limit before the main reflector does. As a consequence, there is a tendency to increase the  $D_S/D_M$  ratio if the above limitation needs to be circumvented. However, this approach also increases the aperture blockage by the subreflector, causing performance degradation.

Although reasonable variations on the basic Cassegrain antenna geometry of Figure 1 can be implemented, for X-band spacecraft antennas a typical compromise of all the above discussed effects leads to  $D_S \approx D_M/8$  and  $\theta_E \approx 25^\circ$  (this edge angle requires a feed horn with about 19 decibel isotropic [dBi] directivity). Assuming a minimum subreflector diameter of 7 wavelengths, one then concludes that the main reflector of the Cassegrain should be at least 56 wavelengths in diameter.

The two reflecting surfaces depicted in Figure 1 are classical (i.e., a paraboloid and a hyperboloid). As a consequence, the feed directivity must be both sufficiently high to minimize the energy spillover past the subreflector and sufficiently low to maximize the antenna efficiency. An optimum is typically achieved when the feed radiation along the subreflector rim direction is about 11 dB lower than towards the subreflector vertex. As Figure 1 indicates, an obvious difficulty with classical surfaces is the fact that the feed energy reflected by the subreflector

vertex region goes back into the feed instead of illuminating the main reflector. The feed aperture then blocks some of the subreflector scattering, increasing the antenna return loss and reducing its efficiency.

However, to a certain extent this problem can and should be corrected using instead a variation of the Cassegrain called the axially displaced Cassegrain (ADC) geometry [2]. Basically, this modified Cassegrain configuration employs a slightly pointed subreflector vertex that diverts the reflected energy away from the main reflector axis. Ignoring conductivity losses and mechanical errors, in the high-frequency limit the ADC reaches an efficiency of about 83%.

Further efficiency improvement can be obtained by completely departing from classical surfaces and using shaped surfaces [3]. In addition to having a pointed subreflector vertex, shaped surfaces also allow the use of an even higher gain feed. The subreflector can then be illuminated with an amplitude taper significantly larger than 11 dB, reducing the spillover to a small level while simultaneously achieving a near-uniform main-reflector illumination. Since with shaped surfaces about 98% efficiency can be achieved in the high-frequency limit (again ignoring conductivity losses and mechanical errors, and assuming  $D_s \approx D_m / 8$ ), any high-gain spacecraft Cassegrain antenna should use shaped surfaces.

Now let's return to the design of compact Cassegrain antennas. To better appreciate the difficulties encountered in this endeavor, consider a typical X-band deep-space spacecraft application (lowest operational frequency of 7.145 GHz) with a gain requirement translating into  $D_m = 2400$  mm. This diameter corresponds to about 57 wavelengths at 7.145 GHz, which, as discussed above, is about the minimum diameter for an X-band Cassegrain. Although this conclusion is somewhat open to dispute, the example should nevertheless clearly indicate that designing small, efficient Cassegrain antennas (e.g., with  $D_m = 1500$  mm) is not a simple task. With such a small subreflector, the unavoidable diffraction effects will significantly reduce the Cassegrain antenna efficiency. Although

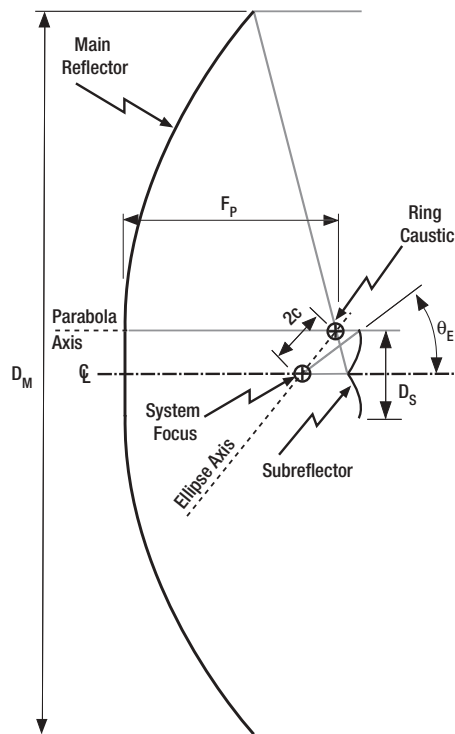
in this situation shaped surfaces will still provide some efficiency improvement, the control of the main-reflector illumination is severely compromised, and the benefits of a pointed subreflector vertex become almost insignificant. Furthermore, since the feed horn dimensions cannot be reduced as the antenna dimensions are scaled down, the blockage caused by the feed horn quickly becomes a significant problem. Clearly then, a different reflector antenna geometry is needed for compact reflector antenna applications.

Since the minimum subreflector size provides one of the dominant limitations of electrically small Cassegrain antennas, an obvious alternative would be to remove it and place a low-gain feed horn at the paraboloidal main reflector focus. This alternative—the paraboloidal reflector antenna—is widely used in many antenna applications and is well covered in the available literature. However, it also has its own limitations when used to implement compact, high-gain spacecraft antennas. In a nutshell, two main difficulties stand out: first, it is very hard to efficiently illuminate paraboloidal reflectors of small relative depth (i.e., small  $F/D$  ratios) due to the lack of high-performance feed horns capable of producing the required broad-angular radiation; and second, a single reflecting surface limits the design flexibility. As a consequence, this alternative also does not produce a highly efficient antenna.

### **The ADE Antenna and Its Advantages**

An alternative dual-reflector antenna design that minimizes several of the problems discussed above is the ADE geometry (shown in Figure 2 together with a few relevant rays). Although this antenna was originally proposed nearly forty years ago [4], its use in compact, high-gain spacecraft antenna applications has only begun to be exploited in relatively recent times. The basic characteristics of this antenna configuration, as well as its design procedure, have recently been discussed in the literature [2]. Its main reflector is produced by spinning an offset section of a parabola, of focal length  $F_p$ ,

Figure 2.  
ADE antenna  
geometry.



about the antenna axis of symmetry. This creates a main reflector with the ring caustic shown in the figure. To appropriately illuminate this main reflector, a subreflector with a coinciding ring caustic and a focus (the system focus) is needed. This can be achieved starting with a displaced section of an ellipse with tilted axis and interfocal distance  $2c$  (hence the name ADE), and spinning this ellipse about the antenna axis of symmetry. The final geometry produced by this process is the ADE antenna.

Observing Figure 2 one notes two outstanding features of the ADE antenna. First, the subreflector has a pointed vertex that directs the feed radiation along the antenna axis towards the main-reflector rim. This assures minimum reflection of energy towards the feed horn, even when the subreflector diameter  $D_s$  is relatively small in terms of the operation wavelength. And second, the illumination of the main reflector central region comes from the feed rays that reflect near the subreflector rim, which also stay away from the region occupied by the feed horn aperture. In sharp contrast with the virtual focus of the Cassegrain geometry (see Figure 1), the ring caustic of the ADE allows the feed horn to move closer to the

subreflector without significant deleterious blockage effects, as the overall dimensions of the antenna are scaled down as needed to produce a compact geometry.

Another significant characteristic of the ADE geometry becomes evident when ray-tracing techniques are used to obtain the aperture field [2]. In the high-frequency limit, and ignoring conductivity losses and mechanical errors, efficiencies around 91% can be obtained without shaping, with  $D_s \approx D_M / 10$  and  $\theta_E$  values in the  $20\text{--}60^\circ$  range, provided that an appropriate taper towards the subreflector rim is used (i.e., between 20 and 12 dB, respectively). Furthermore, again in the high-frequency limit, the ADE efficiency increases as the  $D_s/D_M$  ratio decreases, further favoring compact antennas with small subreflectors.

Although the above characteristics indicate that the ADE geometry is a strong candidate for compact, high-gain antennas, it is well known that the high-frequency limit performance predictions become increasingly less reliable as the electric dimensions of the antenna are reduced. Hence, in order to provide reliable performance predictions, numerical tools based on rigorous electromagnetic analysis techniques were developed to analyze the performance of generalized classical, axially symmetric, dual-reflector antennas and applied to model ADE antennas [5]. The results obtained confirmed the expectations, and were further validated by the ADE demonstration model discussed in the next section. As a side note, work on improving these numerical analysis tools have continued under IND support until fairly recently, producing the tools currently being heavily used to assist in the design and analysis of the MRO X- and Ka-band ADE antenna.

### Compact X-Band ADE Antenna Demonstration Model

A prototype X-band ADE was constructed and measured in order to confirm the outstanding electric characteristics of this antenna geometry for compact, high-gain spacecraft antenna applications. Since this antenna was also designed targeting a particular mission (i.e., the Mars Surveyor

2001 program), it incorporated a few mission-specific constrains that unfortunately reduced its final gain. However, this fact did not significantly detract from the prototype's usefulness as an ADE demonstration and validation model.

The antenna (shown in Figure 3) was designed to operate in both receive and transmit deep-space spacecraft communication bands (center frequencies of 7.167 GHz and 8.420 GHz, respectively). It has an aperture diameter  $D_M=1250$  mm, and a subreflector diameter  $D_S=140$  mm, which are only about 30 and 3.3 wavelengths at the lower operation frequency, respectively ( $D_S \approx D_M/9$ ). In fact, Figure 2 is a scale drawing of this antenna. The subreflector illumination is provided by a simple, two-corrugations, corrugated horn with about 14 dBi gain and  $-23$  dB return loss. This return loss value does not change significantly when the horn is placed in the reflector system, since the subreflector backscattering into the feed is very small in the ADE geometry. The subreflector was supported by a tripod that provided two choices of main-reflector attachment points: at the rim and at  $2/3$  radius (the figure depicts the struts at their  $2/3$ -radius attachment position). Calculations indicated that



Figure 3. ADE antenna prototype (subreflector and feed detail on the insert).

about 0.2 dB gain reduction is produced by the subreflector supports, in either one of the two attachment choices (this positional insensitivity was confirmed by measurements).

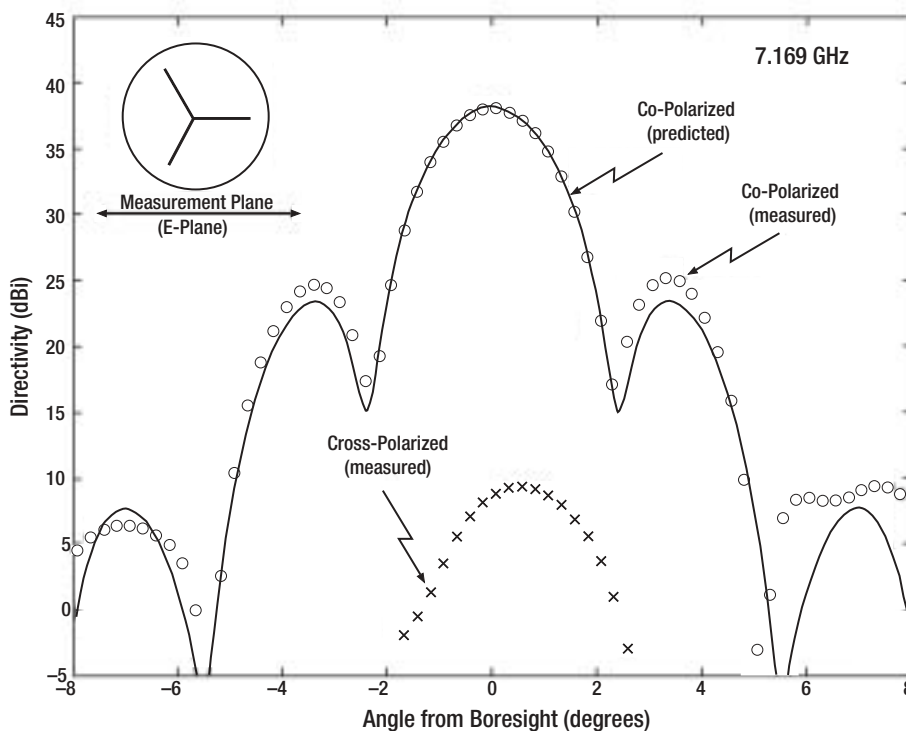


Figure 4. Prototype ADE antenna radiation pattern (insert shows antenna aperture with supporting struts).

With the exception of the subreflector supporting struts, the complete antenna (including feed horn) was modeled using the rigorous numerical tools mentioned in the previous section. The predicted directivity of the antenna was 38.0 dBi and 39.3 dBi, at 7.167 GHz and 8.420 GHz, respectively (ignoring mechanical errors, strut effects, and conductivity losses). This corresponds to efficiencies of 70% and 72%, respectively. The measured gain results agreed well with these numbers once the impact of mechanical errors, ohmic losses, and strut effects were accounted for (within an estimated probable measurement uncertainty of  $\pm 0.5$  dB). Typical predicted and measured radiation pattern results are shown in Figure 4. They demonstrate the quality of the agreement that can be expected when the developed numerical tools are used to model ADE antennas. The cross-polarization shown is a measurement artifact, and the discrepancies observed in the sidelobes are attributed to the scattering produced by the subreflector supporting struts as well as to mechanical inaccuracies.

### Summary and Conclusion

The basic characteristics that render the ADE attractive for compact, high-gain spacecraft communication applications have been reviewed and compared to the corresponding characteristics of the ubiquitous Cassegrain antenna geometry. In contrast with the Cassegrain, the ADE geometry allows the implementation of considerably smaller apertures (i.e., diameters of 30 wavelengths or less) while yielding higher efficiency. The predicted and

measured results of an ADE validation and demonstration prototype were presented. They confirm the excellent performance that can be expected from this antenna configuration.

### Acknowledgements

Mr. Dana Lafavour and Mr. Arthur Dahlberg (Boeing Satellite Systems, Seattle) conducted the mechanical construction and the electric measurement of the compact ADE demonstration model, respectively. The support of Ms. Suzanne Spitz (JPL) was instrumental in the ADE antenna demonstration model development.

### References

- [1] P. W. Hannan, "Microwave antennas derived from the Cassegrain telescope," *IRE Trans. Antennas and Propagat.*, vol. AP-9, pp. 140-153, Mar. 1961.
- [2] F. J. S. Moreira and A. Prata, Jr., "Generalized classical axially symmetric dual-reflector antennas," *IEEE Trans. Antennas and Propagat.*, vol. AP-49, pp. 547-554, Apr. 2001.
- [3] V. Galindo, "Design of dual-reflector antennas with arbitrary phase and amplitude distributions," *IEEE Trans. Antennas and Propagat.*, vol. AP-12, pp. 403-408, Jul. 1964.
- [4] J. L. Lee, "Improvements in or relating to microwave aerials," U.K. Patent 973 583, Oct. 1964.
- [5] F. J. S. Moreira, "Design and rigorous analysis of generalized axially-symmetric dual-reflector antennas," Ph.D. dissertation, Univ. of Southern California, Los Angeles, CA, Aug. 1997.



# Low-Thrust Spiralling Trajectory Design

## Introduction

The commonly-used term “low thrust” is a modest one, for it does not capture the highly efficient use of propellant typically possible with low-thrust propulsion devices. For example, various types of electric propulsion, when compared with chemical rockets, offer ten-fold or greater gains in propulsive efficiency. The “low thrust” of low-thrust devices arises because propellant can be expended only slowly, when compared to chemical rockets. This thrust, however, can be applied over long periods of time. The ion thruster on the Deep Space 1 spacecraft supplied thrust for a total of almost 2 years, as compared to thrust-durations of minutes for chemical rockets. On balance, certain missions can benefit from such low-thrust propulsion. For example, NASA’s upcoming Dawn mission, which is to orbit two asteroids in succession, could not have met Discovery-class constraints had it used chemical rather than electric propulsion.

From a trajectory design perspective, the challenge of using low-thrust propulsion lies in deciding when and in which direction to apply thrust. The challenge is especially acute for low thrust-to-weight ratios, which produce spiralling trajectories involving many revolutions around the central body. In this case, even just the numerical integration of the equations of motion for a *given* thrust-profile can require significant amounts of time, making it impractical to use traditional optimization techniques (that require thousands of integrations) to determine an *optimal* thrust profile.

In this article we mention new techniques and algorithms, both analytical and numerical, for obtaining efficient, many-revolution, low-thrust orbit transfers, and

escape or capture spirals. These advances, while particularly useful in preliminary mission design studies, can also serve as starting points in optimization or in higher-fidelity computations.

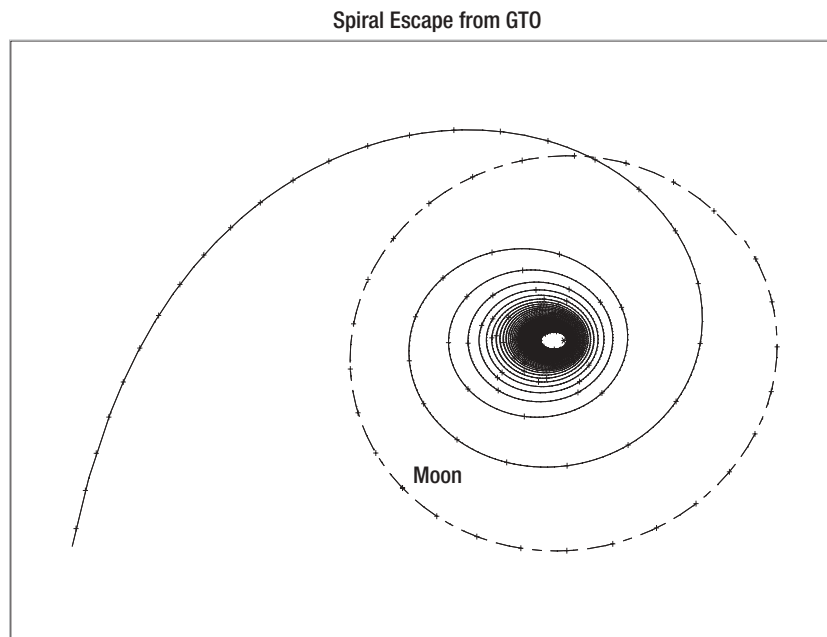
## Escape and Capture Spirals

To escape in minimum time from orbit around a body (or, conversely, to capture to it) requires the low thrust to be applied continuously. In this case, thrust along the velocity vector (or against it for capture) is close to the optimal thrust direction for minimum time [1]. Figure 1 shows such a tangential-thrust escape from geostationary transfer orbit (GTO). Almost 94 revolutions are needed to escape, most of them occurring well below the Moon’s orbit, where they are so close together as to be indistinguishable from their neighbouring revolutions on the plot. The perturbing effects of the Sun and Moon are insignificant on these inner revolutions.

In the past, time-consuming numerical integration was required to estimate the propellant cost for minimum-time escape spirals starting from elliptic orbits. Analytic estimates were available only for near-circular starting orbits. GTO, for example, has an eccentricity of about 0.73, well outside the range of applicability of these earlier estimates. Based in part on the technique of orbit averaging, we have developed new analytic estimates of propellant costs that are applicable to all eccentricities from zero to almost one, and for all thrust-to-weight ratios [2]. In addition, the evolution of the orbit with time is also available. The new analytic estimates allow the performance of a wide range of cases to be assessed rapidly. The

Anastassios E.  
Petropoulos

Figure 1.  
Continuous-thrust escape from an initial Earth orbit of 200 km periapsis altitude by 35786 km apoapsis altitude (geostationary transfer orbit).



more promising cases can then be passed on to higher-fidelity or optimization analyses.

In optimization, for example, one can ignore the inner revolutions, since they add a significant computational burden while offering little potential for improvement over the analytic estimates, and instead focus on using the perturbing effects of the Sun and Moon to advantage. These effects are significant only on the last five to ten revolutions, and so only this outermost portion of the spiral need be included in the optimization. The optimization software, *Mystic*, based on Static/Dynamic Control [3], has been used successfully to compute many such spirals as parts of more complex trajectories [4]. Figure 2 (courtesy G. Whiffen) shows an escape spiral with coast arcs, starting in high Earth orbit. Two close approaches to the Moon facilitate the escape, with the effect of the first flyby significant enough to be clearly visible on the trajectory plot. This escape spiral is just the first part of a single, fixed-time, propellant-optimal, low-thrust trajectory that rendezvouses at Mars.

### Orbit Transfers

The case of continuous tangential thrust described above, while suitable for escape or capture, is of only limited use in the general orbit transfer problem, as the orbit evolves in a single predetermined way, not allowing any flexibility in the initial and final orbits.

Indeed, any of the six orbit elements may need to be changed during an orbit transfer. We are developing judicious control laws, which may include coast arcs, to effect such orbit transfers.

An example of a newly developed control law is for transfers involving a plane change as well as a change in semi-major axis. Figure 3 shows a transfer from a 1000-km altitude, circular, equatorial Earth orbit to a 3600-km altitude, near-circular, polar orbit. The initial and final orbits are shown in bold, with the initial orbit lying in the x-y plane. For illustrative purposes, a relatively high thrust-to-weight ratio has been used to avoid the appearance of closely spaced revolutions that would obfuscate the orbit transfer on the plot. At lower ratios, the revolutions would follow the same general trend, but they would be more numerous and more closely spaced. It is easier to change the inclination of larger orbits. For the large plane change required here it is more efficient to enlarge the orbit well beyond the target orbit size, accomplishing the majority of the plane change at the larger orbit prior to returning to the required final orbit size. Indeed, in Figure 3 the first revolutions are devoted mostly to enlarging the orbit, with most of the plane change clearly occurring at the larger orbits. The final revolutions are then used mostly for returning to the desired orbit size.

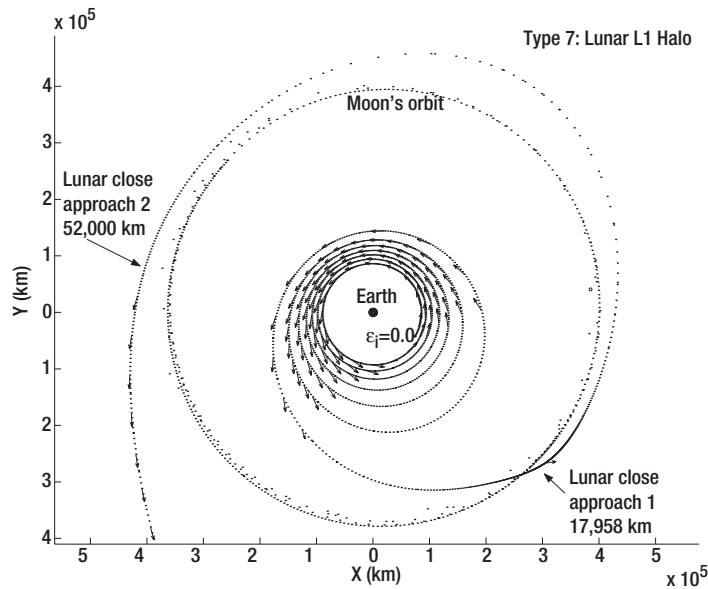


Figure 2. Earth-escape portion of a low-thrust, propellant-optimal Earth-Mars rendezvous trajectory (courtesy G. Whiffen). Arrows are indicative of thrust.

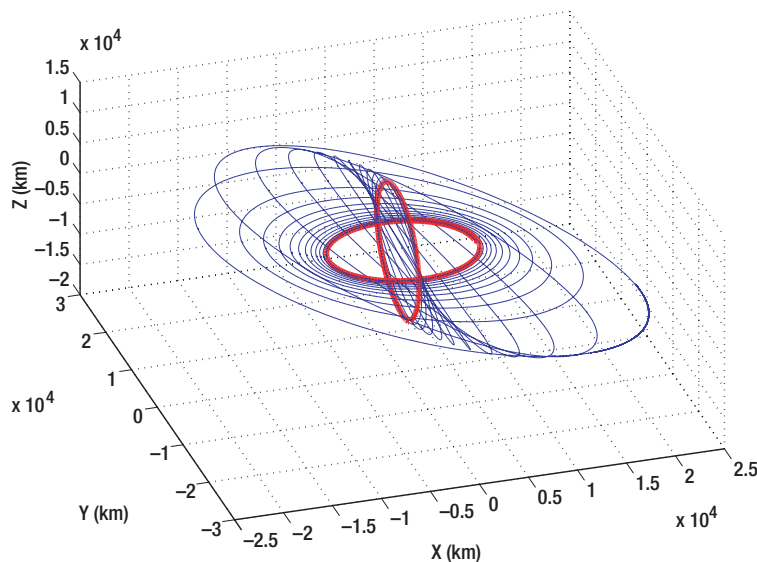


Figure 3. Low-thrust orbit transfer with 90° plane-change and 2600-km altitude gain.

## Conclusions

The new techniques and algorithms we are developing will enable effective trajectory design for new classes of missions, namely those using low thrust to enter, leave, or transfer between different orbits around targets of scientific interest.

## References

- [1] A. E. Petropoulos, G. J. Whiffen, and J. A. Sims, "Simple control laws for continuous-thrust escape or capture and their use in optimisation," AIAA/AAS Astrodynamics Specialist Conference, AIAA Paper 2002-4900, Monterey, California, Aug. 5–8, 2002.
- [2] A. E. Petropoulos, "Some analytic integrals of the averaged variational equations for a thrusting spacecraft," in *IPN Progress Report* 42-150, Aug. 15, 2002. Available: [http://tmo.jpl.nasa.gov/progress\\_report/42-150/150H.pdf](http://tmo.jpl.nasa.gov/progress_report/42-150/150H.pdf)
- [3] G. J. Whiffen and J. A. Sims, "Application of a novel optimal control algorithm to low-thrust trajectory optimization," AAS/AIAA Space Flight Mechanics Meeting, AAS Paper 01-209, Santa Barbara, California, Feb. 11–15, 2001.
- [4] G. J. Whiffen and J. A. Sims, "Application of the SDC optimal control algorithm to low-thrust escape and capture trajectory optimization," AAS/AIAA Space Flight Mechanics Meeting, AAS Paper 02-208, San Antonio, Texas, Jan. 27–30, 2002.



# Simulation Tools for Protocol Design and Evaluation

Jay L. Gao

## Introduction

A properly designed communication protocol can provide important data transfer services and cost-saving automation for complex operations such as connection establishment and termination, quality of service (QoS) negotiation, error control, link outage recovery, adaptive reconfiguration, and application-level information management. Protocol development can be described generally as a process alternating between design and performance evaluation activities. At the initial stage of development, analytical methods are often used for proof-of-concept and coarse-grain evaluation of potential improvement in the system performance. If the original design concept shows validity and potential for performance enhancement, further refinement of the protocol design and subsequent performance evaluation will take place. As this process unfolds, many simplifying assumptions will be replaced by practical constraints and details. Eventually, the behaviors of the communication protocols, under the influence of nonstationary stochastic phenomena such as fluctuating channel qualities and dynamic traffic generated by autonomous science applications, will become highly nonlinear and intractable to analysis. Therefore a simulation-based approach becomes critical. It will provide the vital tool necessary for comparing the pros and cons of different protocol features and services. Strengths and weaknesses of the design are revealed under a variety of application scenarios, so that development effort can be strategically focused. Such a modeling and evaluation tool can also provide the necessary data for return-on-investment (ROI) analysis on a

protocol's contribution to the overall system performance.

## Lander-Orbiter Link Simulation

As a task under the IND Technology Program, a simulation tool with all the associated software models for space-based communication protocols, such as the Proximity-1 space link protocol, etc., has been developed for the purpose of evaluating communication network performance for NASA's space/planetary missions. Initial effort focuses on the lander-orbiter link in the context of Mars exploration, with future extension aimed at the complete end-to-end simulation the Mars Relay Network as well as other space/planetary missions.

A lander-orbiter communication link is a complex, dynamic system. Planetary and spacecraft motion creates episodic connectivity within the network, and the time-varying geometry, including the antenna gain pattern, spacecraft orientation, and slant range, constantly changes the quality of the communication link. To a very high degree, these phenomena can be modeled accurately with existing tools, such as the Satellite Orbit Analysis Program (SOAP), that have analytic models of orbital geometry and link budget calculation. However, other nonstationary stochastic phenomena, such as multipath fading and atmospheric effects on the radio channel, cannot be described adequately as a constant mathematical factor in the link budget. Lacking a better understanding of how a communication system, using particular protocol features, will perform under the influence of these random phenomena, a link margin is typically added to the system overhead in order to guarantee the worst-

case performance. The result is often over-provisioning of resources at the expense of system performance.

The result of an ultrahigh-frequency (UHF) field experiment [1] conducted at Stanford University shows that a significant gap exists between the actual radio channel condition and its geometrically derived prediction. It also clearly demonstrates the importance of designing real-time channel-adaptive techniques. These techniques can dynamically adjust link margin to take advantage of the high-gain period and compensate for the low-gain period during a pass. This is using predetermined configuration(s) based on results generated from geometric prediction models alone, which would entail the usage of large link margin since the prediction result is not sufficiently reliable. A statistical model that accurately describes the behavior of the radio channel and a high-fidelity simulation of the interaction between the protocol and the radio channel are important for the optimization of current protocol configuration and the design and development of additional real-time channel-adaptive features.

The near-term goal of our lander-orbiter link simulation is to predict the performance of Mars in-situ communications using the Consultative Committee for space Data Systems (CCSDS) Proximity-1 link protocol under different configurations and conditions. Various protocol options, such as expedited vs. reliable services, half-duplex vs. full-duplex mode, and variable vs. fixed data rate schemes are evaluated for their impact on the system as measured by conventional performance metrics such as total telemetry bits return and QoS metrics based on the existences of “gaps” and “error” in the delivered data or latency.

### **Modeling Approach and Description of the Simulation Tool**

We model three distinct components in the lander-orbiter communication by interfacing different analytical and simulation tools. The three components are (1) the orbital geometry of the deployed network, (2) the physical channel characteristics and communications link engineering, and (3)

protocol behavior and traffic generation process. A four-step procedure for performance evaluation is shown in Figure 1.

The first step of the process is to model the geometric aspect of the deployed network. We use the SOAP tool to calculate the slant range and connectivity of the lander-orbiter link as a function of time based on orbital ephemerides. The SOAP tool provides an estimate on the received signal strength for the lander-orbiter link as a function of time through a simple link budget calculation that also account for path fading and antenna patterns.

In the second step of the process, the results generated by the SOAP tool are time-stamped and stored in files that are then imported into a channel characterization tool, written in MATLAB code. The code refines the link quality characterization by incorporating factors such as channel gain fluctuation due to multipath fading and atmospheric scintillation, background noise, and link engineering parameters such as modulation and data rate. The MATLAB tool can generate a stochastic profile of a communication link in the form time-varying signal-to-noise ratio (SNR) or bit error rate (BER) processes.

In the third step, the SNR or BER profile is provided, along with propagation delay, fixed or variable data rate process, and the link schedule, to the QualNet-based network simulation engine. This engine models the state transition logic and algorithms executed by the communication protocol as it processes incoming and outgoing information data units.

In the fourth step of the procedure, performance metrics such as throughput, latency, buffer utilization, energy consumption, and other QoS metrics are computed and visualized by the QualNet graphical user interface (GUI).

### **Example Scenario: MER-Odyssey Link Performance Evaluation**

In this section, we will illustrate the use of our simulation tool to model MER-Odyssey communication using the Proximity-1 space link protocol in detail and evaluate the

Figure 1. Four-step procedure for performance evaluation.

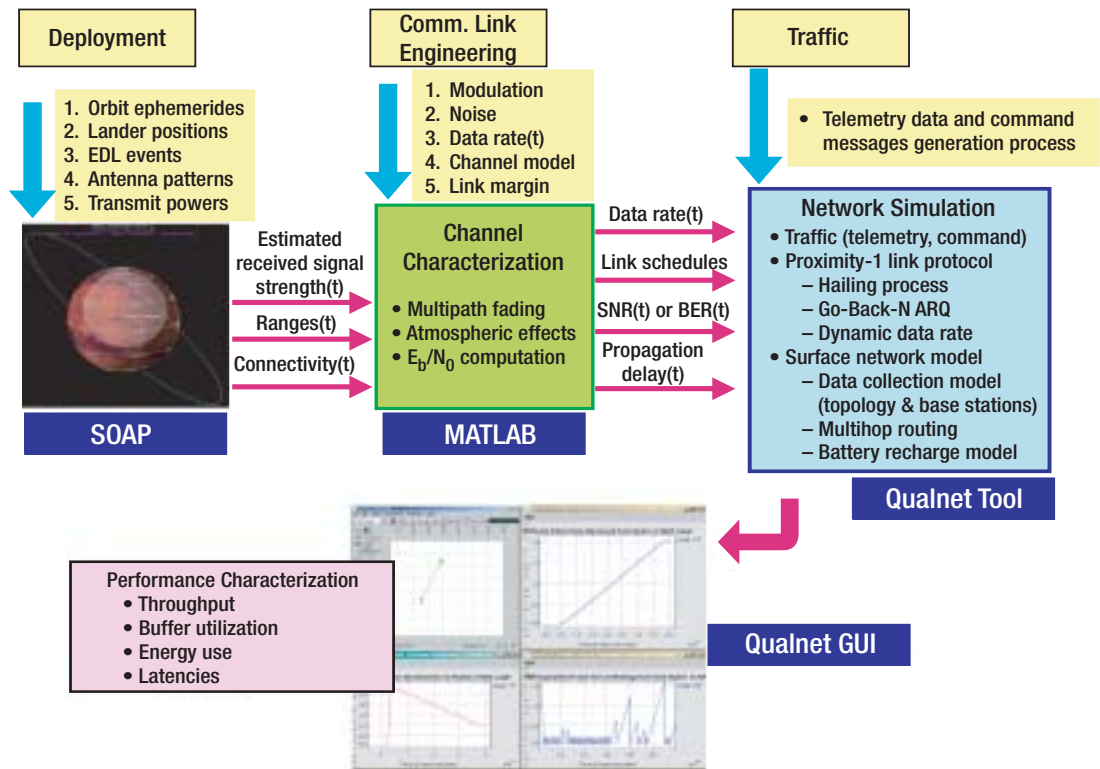
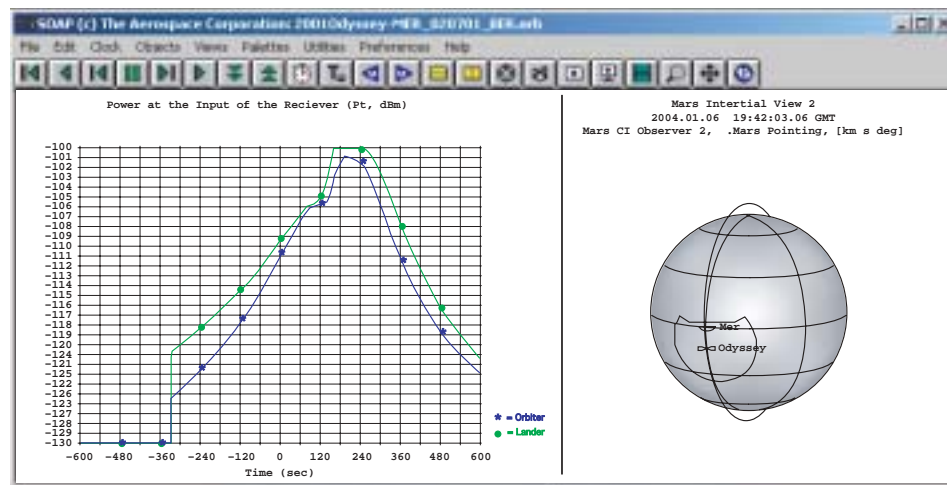


Figure 2. MER-Odyssey UHF link signal stress profile.



system performance and QoS metrics under a variety of link configuration and traffic loading scenarios.

Following the four-step procedure described in the last section, the evaluation process began by modeling the geometric aspect of the deployed network. In this example, the MER-Odyssey relay geometry is modeled, and the received signal strength as a function of time is estimated for a 6-minute pass. Although a single pass is chosen for simplicity in this illustration, the

simulation tools can easily study multiple passes without additional complexity in the evaluation procedure. Figure 2 shows the received signal strength profile for the forward and return links as a function of time.<sup>1</sup>

<sup>1</sup>From an Earth perspective, the term "forward" is synonymous with communication from "orbiter to lander" or Odyssey to MER and "return" is synonymous with communication from "lander to orbiter" or MER to Odyssey.

To properly characterize the radio channel and link performance, factors such as link margin, noise floor, noise figure, modulation index, data rate, atmospheric scintillation, and multipath fading are incorporated with the result generated by SOAP using MATLAB. Link-engineering parameters are extracted from Odyssey's design document [2]. In addition, a uniformly distributed random process, whose magnitude is upper-bounded by the chosen link margin for Odyssey, is superimposed on the received signal strength data to synthesize the expected random variation in channel gain. The MATLAB tool computes the Eb/No values as a function of time and generates the BER profiles for the 6-minute pass at different data rates ranging from 128 to 512 kilobits per second (kbps.)

Figure 3 shows samples of the MER-to-Odyssey BER profile generated for a 6-minute pass at 128, 256, and 512 kbps. The horizontal line marks the  $10^{-6}$  threshold, below which one would consider the channel to be "reliable." We can see that as data rate increases, the BER shows considerable fluctuation above the  $10^{-6}$  threshold during the pass.

The third step of the procedure is to simulate the lander-orbiter communication process when using the Proximity-1 protocol. Two nodes are created in the QualNet simulation environment to represent MER and Odyssey and configured to simulate its link-layer communications using the Proximity-1 protocol. Figure 4 shows a screen shot of the QualNet simulator. The four windows show, in clockwise order starting from the upper-left corner, the network topology, the number of received data frames, the waiting time process of orbiter with respect to the expedited data stream, and the transmission buffer size, as measured by the number of frames, at the lander. A script file containing the communication schedule for the 6-minute pass is read by the simulation engine to trigger the appropriate protocol actions such as hailing (link establishment), data communication, and link termination. The QualNet simulation engine reads the BER profile of the channel from a separate text file.

QualNet's built-in application-layer models provide the ability to generate data traffic for the scenario. We assume the data buffer holds enough data to fill the entire 6-minute pass, and all data frames have fixed payload size of 1 kilobyte. Two types of traffic are serviced simultaneously during the 6-minute, Promity-1 link pass: (1) reliable traffic, such as science data that requires "reliable" QoS, i.e., gap-free and error-free delivery, and (2) expedited traffic, which is generated during the pass at regular time intervals and often has a tighter latency requirement, though it may

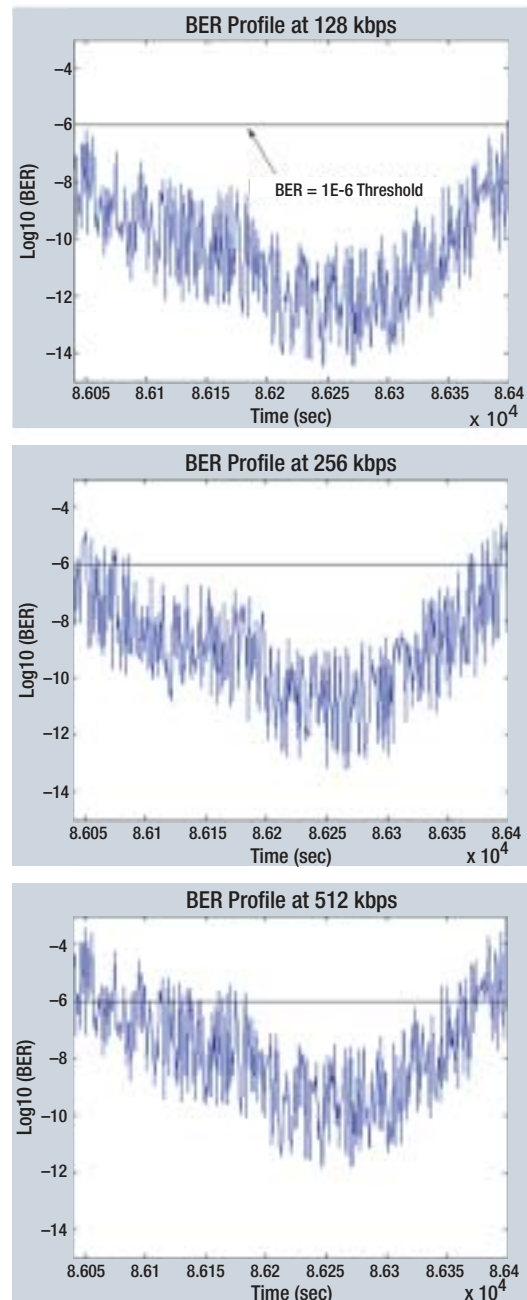
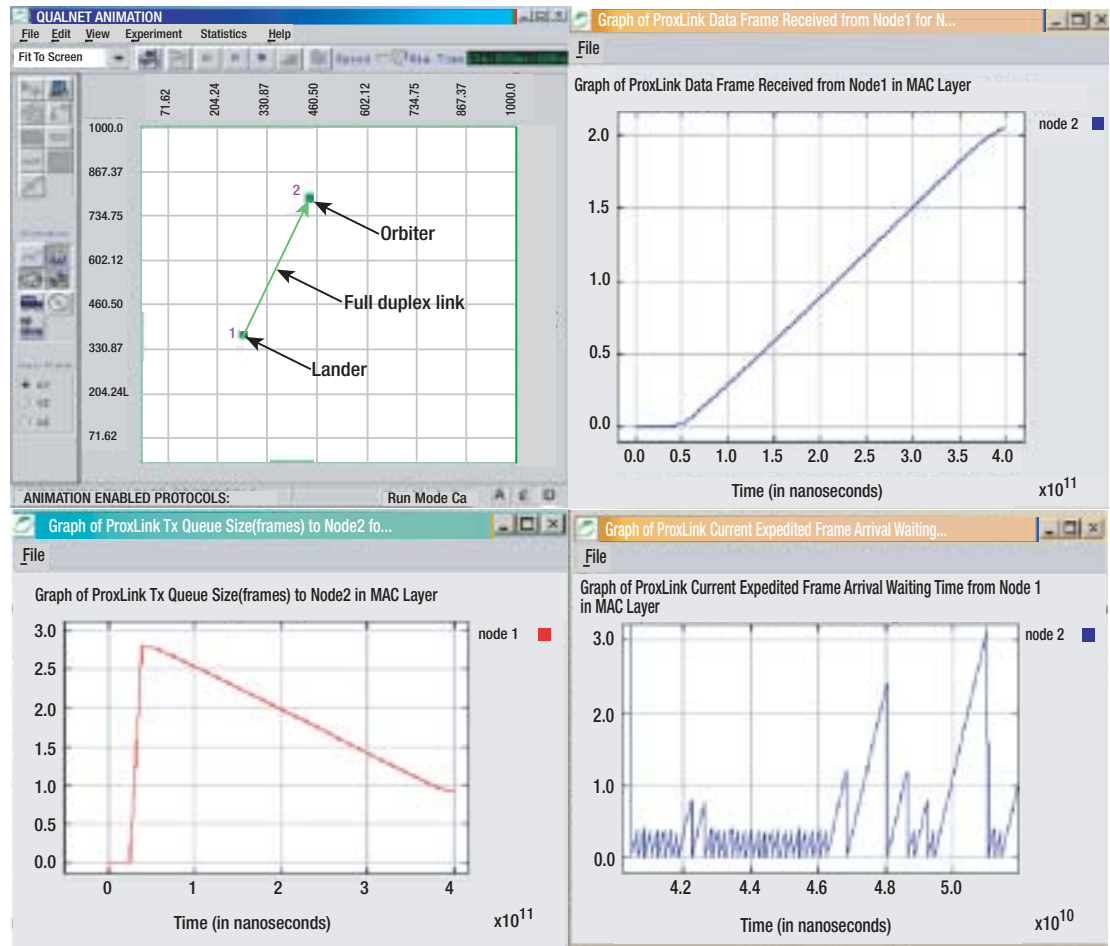


Figure 3. MER-to-Odyssey BER profile for a 6-min pass at 128, 256, and 512 kbps.

Figure 4. QualNet simulation of MER-Odyssey Proximity-1 link.



not require a delivery guarantee. Examples of this second class of traffic could be engineering or navigation data whose QoS is measured by the “timeliness” or “flow” quality in data delivery, instead of by the total data volume or the occurrences of errors and gaps. Proximity-1 protocol provides automatic repeat request (ARQ) services for only the reliable data stream, but the expedited streams are given higher queuing priority for

channel access due to their tighter restriction on latency. We assume that the reliable data is generated by the MER rover and is queued into the transmission buffer at a rate of 16 megabits per second (Mbps), 15 seconds prior to the beginning of the pass. The expedited data stream has the same frame size, and one frame will be generated every 200 milliseconds during the pass. Table 1 summarizes the performance of the Proximity-1 protocol,

Table 1. Simulation results.

Data Rate		128 kbps	200 kbps	256 kbps	320 kbps	512 kbps
Minimum Link Margin		5 dB	3.04 dB	2 dB	1.03 dB	-1 dB
Instantaneous Max BER		$1.5 \times 10^{-6}$	$7.3 \times 10^{-6}$	$2.7 \times 10^{-5}$	$5.2 \times 10^{-5}$	$9.2 \times 10^{-4}$
Reliable	Tx Frames	3738	6853	9276	12045	20352
	ReTx Frames	0	9	113	214	1562
	Total Data Return (Mbits)	29.9	54.8	73.3	94.6	150.3
	Average Frame Latency* (sec)	194.15	193.4	192.07	192.05	191.2
Expedited	Tx Frames	1800	1800	1800	1800	1800
	Lost Frames	0	3	6	8	74
	P (W>600 msec)	0	0	0	0.0027	0.0157

\* Only counts frames that are transmitted and received within the 6-minute pass.

servicing multiplexed, expedited, and reliable data streams at different data rates.

In this case we can see that while increasing the data rate (which reduces the link margin) will increase the BER, the reliable data stream can still be delivered above the  $10^{-6}$  threshold due to the application of ARQ error control. Thus, as long as the BER is not too large to maintain physical channel synchronization, link margin should be relaxed to maximize the total data return. However, when the reliable stream is multiplexed with the expedited data stream, which has tighter latency constraints, lower link margin may hurt the expedited traffic QoS, which in our case is defined as a probabilistic bound on the “waiting time”  $W$ . The waiting time  $W$  is a random variable defined as the time interval between any arbitrary time instance within the pass and the last expedited frame received prior to that time instance. So if we pick an arbitrary time  $t$ , then  $W(t)$  is the time between  $t$  and the last expedited frame received prior to  $t$ . Since  $t$  can be any time instant within the pass,  $W$  is a random variable. The waiting time QoS metric provides a measure of the “timeliness” or “flow” of data delivery, which is important for real-time traffic such as spacecraft engineering data or navigation control traffic. If we set the QoS criteria such that  $P(W > 600 \text{ msec}) < 0.01$ , then clearly 320 kbps, not 512 kbps, is the best data rate for both maximizing the reliable data return and meeting the expedited traffic QoS constraint. Figure 5 shows the waiting time statistics collected by the simulation.

## Conclusion

We have described a simulation tool developed under the IND Technology Program and demonstrated its capability for detailed, high-fidelity communication modeling and performance evaluation for NASA’s space/planetary missions. This tool not only helps to optimize the protocol configuration under different mission scenarios, it also provides the protocol developers with a realistic assessment of the relative merit of various features, services, and configuration options. Such modeling

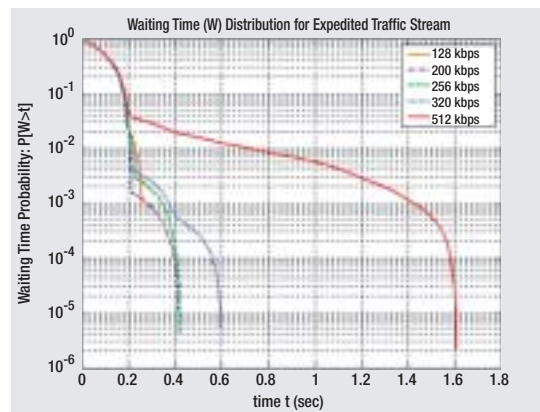


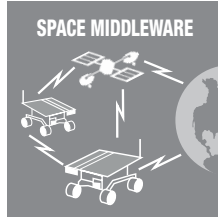
Figure 5. Waiting time statistics for expedited traffic.

and simulation could lead to the addition and refinement of certain protocol functionalities, and the removal of those features that do not provide sufficient performance improvement and/or ROI.

Ongoing efforts in our simulation tool development include building models for other higher-layer space-based protocols such as the CCSDS File Delivery Protocol (CFDP), enabling alternative modeling of complex physical phenomena through a hybrid continuous-time/discrete-time coupling of the simulation platform with laboratory/field experiment data, and extending the current scenario toward a complete end-to-end multihop network simulation of the Mars Relay Network and other space/planetary mission scenarios. Also, we are working on developing additional features in the channel characterization tool that can synthesize multipath fading effects based on a user-specified power spectrum density vector.

## References

- [1] M. Danos, A. Barbieri, and A. Vainys, “MER Rover UHF Antenna Field Tests,” JPL-IOM 3312-02-0001, October 2001.
- [2] *2001 Mars Odyssey: Relay Data Service*, JPL D-19501, PD 722-803, Rev. A, April 2001.



# Space-Based Middleware Technology

*Norman  
Lamarra*

## Abstract

The commercial Internet is evolving service-oriented capabilities to enable new kinds of distributed applications in business, engineering, and management. A current buzzword in this domain is “web services”, representing a standardized approach to deploying distributed applications whose software components and data sources may be in different locations, formats, languages, etc. Distributed applications are less mature in the space exploration domain, but the potential is equally dramatic. We believe appropriate middleware technology can enable near-term space missions to leverage resources (sensors, processing, analysis, etc.), but in the longer term can lead to an entirely different space network. We further believe that a service-oriented architecture is key, and could be incrementally deployed in space, contributing to the evolution of increasingly capable, efficient, and eventually autonomous remote exploration. In turn, this could provide higher-quality science with lower operations cost, and make each mission simpler and more robust, hence reducing risk. Such a service-based architecture could simplify access to information such as navigation, weather, terrain, and remote computation, and (as in the Internet) would become progressively more useful as more services are deployed and as more craft collaborate. Like web services, participation in middleware technology can be made extremely simple (even supporting low-cost sensor web micro-units), while allowing resources such as bandwidth and storage to be much more effectively leveraged (e.g., between a fixed micro-sensor, rover, and orbiter).

Further into the future, this approach could assist participants to produce or consume information at various levels, via adaptive software agents (e.g., sensor processing controlled by the investigator to report only on features deemed interesting). Initially, however, we expect middleware to simplify automation, both in space and on the ground, by implementing standards designed to simplify interoperability and cross-support, including standard communication protocols.

## Introduction

Middleware can be viewed as any software involved in connecting separate application pieces (components). The result can be either a single distributed application or a collection of cooperating stand-alone applications (in which case the components are actually complete applications). Commercial middleware technology has evolved steadily over the last 10 years, much of it related to Internet technologies. Some reasons for using the component approach in distributed applications include the following:

- Components can be separately developed and can be on different platforms
- Components can be reused in different applications
- Components can make applications more robust
- Overall performance can be improved by tuning component usage (e.g., a server component can be replicated to increase capacity or manage loading)
- Applications built from smaller components may be easier to develop, deploy, maintain, and adapt than are monolithic applications.

There are several further advantages to be gained by *standardizing* middleware (integrating such components)

- Use of standard interfaces can simplify software development by avoiding reimplementations of similar functionality for different applications (e.g., open database connectivity, or ODBC)
- Language dependency can be mitigated (by providing bindings for the same interface in different languages)
- Interoperability is easier to achieve and verify.

And all of the above should significantly reduce cost. However, there are also some potential pitfalls with the middleware approach, such as:

- Performance can be unexpectedly low (e.g., due to network latencies or inefficient object references)
- Interfaces must be tightly controlled, and sometimes several versions must be supported simultaneously
- Organizational boundaries may impose constraints (e.g., nonownership of “the other piece” may limit one’s choices).

In this context, any infrastructure that enables construction of distributed applications, including technologies such as the common object request broker architecture (CORBA), can be viewed as middleware.

In a layered view, middleware encompasses any software residing “below” the application layer—this could include networking infrastructure or middle tiers between a client application (such as a browser) and a back-end server (such as a database). Recently, standardized middleware has been moving away from tight coupling (i.e., synchronous remote procedure call or remote method invocation) towards looser coupling (i.e., asynchronous message-oriented middleware, or MOM). One of the most recent manifestations of this trend is web services. In this architectural model, application components expose service interfaces that are well defined (by web services description

language or WSDL), and typically accessible using hypertext transfer protocol (HTTP). For example, one component accesses another at a particular uniform resource locator (URL) address via messages that are typically encoded using extensible markup language (XML) rather than HTML. This can be described as enabling dynamic conversations with remote web pages in which application objects are embedded. The objects (which do the actual work) are themselves described and accessed using simple object access protocol (SOAP).

Distributed-system technology was at first mainly focused on business applications residing on the (wired) intranet. Later, application components exposed interfaces to the Internet, for example, to allow customers to order products online. Web services grew as an extension of such customer-provider, client-server applications into a domain where the customer may be viewed as a requesting agent (automated software) and the provider as a service rather than a server. The requirements of automation forced the standardization of interfaces: for example, to continue the purchasing analogy, if there is no human to view, interpret, and fill in a graphical order form, then the order mechanism must be described in a machine-interpretable way. Current trends toward mobility are also driving extension of the web-services approach to the wireless domain. This is a good match, because loosely-coupled MOM is more adaptable to (dynamic) wireless connectivity than is the synchronous approach. Automation is implicit at several levels: applications request network connectivity; networks provide routing capability; and perhaps networks dynamically configure themselves according to traffic patterns, types, or even priority. When we use a cell phone to pick up email, we are probably not aware of how many services are cooperating to deliver it to the display.

In the deep-space domain, however, use of distributed-system technology is many years behind—typically, missions are primarily interested in getting commands from Earth to the spacecraft, and getting

data (health or science) back. They thus typically utilize a point-to-point (though necessarily asynchronous) communications model. We believe that this mindset has precluded bringing many of the middleware benefits from the commercial marketplace (as described above) into the space domain. We believe such middleware is capable of providing enabling (rather than merely enhancing) capability in some situations. In particular, the recent availability of robust MOM provides an approach with even more benefits for the (wireless) space domain than for (wired) local area network (LAN) communications. This is because the former domain typically has longer latencies, intermittent connectivity, and lower bandwidth than the latter, and it is easier to make asynchronous messaging robust than to make synchronous (or blocking) remote calls robust. Finally, since JPL has many missions on its calendar, we believe there is significant payoff in standardizing both the service architecture and the implementation as much as possible.

#### **Vision/Benefits**

In this spirit, an Interplanetary Networking Architecture is being developed, with the aim of leveraging some of the Internet's benefits into the deep-space domain. At a high level, this architecture has proposed using existing successful approaches in local intranet domains where possible (e.g., between different spacecraft at the same planet), while interconnecting such remote intranets via new approaches (e.g., bundling protocols) into a "galactic extranet". This implies that communications *among* several such spacecraft may become more common in the future in addition to the traditional *uplink* and *downlink* used for the "solo" missions of the past. And as seen with the evolution of the terrestrial Internet, standardized protocols (such as the transmission control protocol/Internet protocol, or TCP/IP suite) provide the most effective basis for proliferation of distributed applications. Thus a component of Interplanetary Network Directorate (IND) research is devoted to consideration of the requirements placed on such protocols by the envisioned interplanetary network. Adrian Hooke, Vint Cerf, and other luminaries of the

space and ground communications domains have proposed the name "delay-tolerant protocols" to describe this new class.

Space-based middleware can be viewed as dependent on such protocols in the same sense that terrestrial Web services applications are dependent on Internet protocols. In this view, the primary purpose of such middleware is to enable new service-based application capabilities separately from the applicable communication protocols. For example, CORBA and then Java began in the mid 1990s by leveraging the mature TCP/IP protocol for interorb communication and remote-method invocation respectively. More recently, web services have been configured to ride on several alternate protocols; the simplest is HTTP, but others have been used to provide different benefits. For example, the Java Messaging System (JMS) can provide robustness via its reliability features (retransmission, replication, etc., like TCP) while raw HTTP cannot. In the commercial marketplace, several vendors are implementing messaging standards like message-passing interface, real time (MPI/RT). Others have adapted their own proprietary messaging systems for use in this new web-services domain—for example, IBM's MQseries™ and TIBCO's ActiveEnterprise™ family, among many other products. Figure 1 shows a conceptual architecture built on such middleware for operation in the space domain among orbiters, landers, rovers, craft in formation, and ground stations.

Figure 2 shows how a middleware-enabled "space web" could enable such craft to utilize each others' assets more effectively. The space web could simplify access both to *information* (such as navigation, weather, and terrain) and also to *resources* (such as remote storage, computation, or other assets). An example is the current Internet-based global monitoring and navigation network, which is used for precise orbit determination. The web would become progressively richer as more services are deployed and more craft collaborate, as described in the following examples.

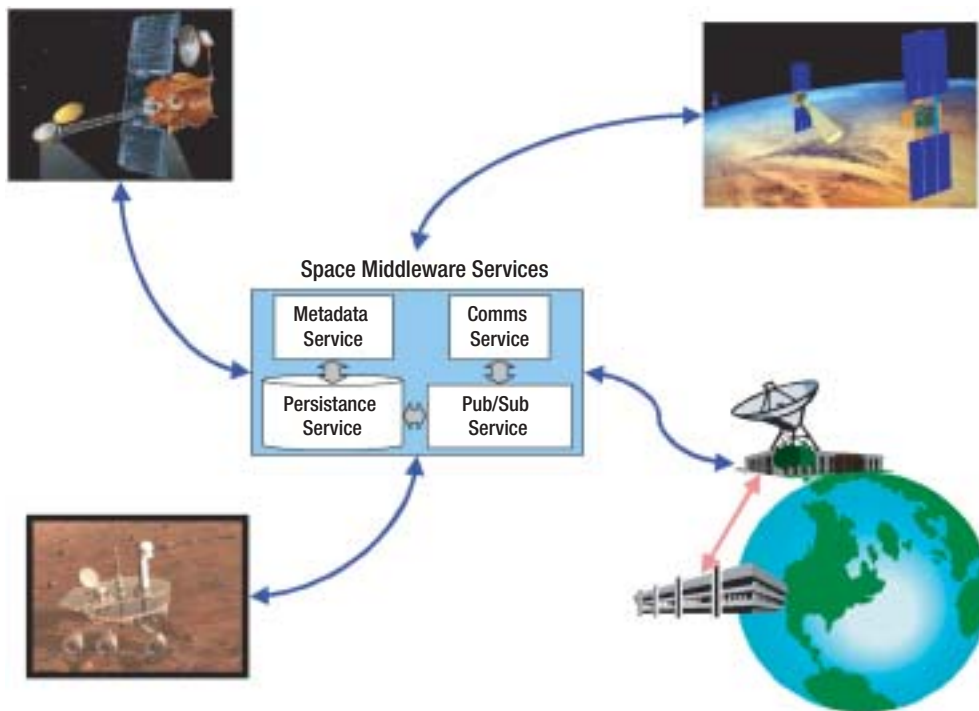


Figure 1.  
Space middleware domain

*Autonomous mobility:* During traverse, a rover could verify its own position observations by receiving mapping information from an orbiting mapping sensor. High-resolution imagery could also help in path planning. If such information could be obtained locally, a round trip to Earth would be avoided, thus improving decision response time and perhaps assisting opportunistic science. Similarly, weather or even computation services (including planning) could be supplied locally rather than requiring Earth involvement. Such local access requires the ability to find and retrieve appropriate data.

*Deep space communication:* Standardized protocols (e.g., those of the Consultative Committee for Space Data Systems, or CCSDS) can help optimize use of constrained resources such as bandwidth, power, etc. However, similar standardization at the application layer could improve use of the communication channel itself, by allowing standard ways for applications to manage and transport data. In addition, lower latency and higher aggregate bandwidth may be available locally among spacecraft than between any one spacecraft and Earth, and middleware could or simplify utilizing such resources.

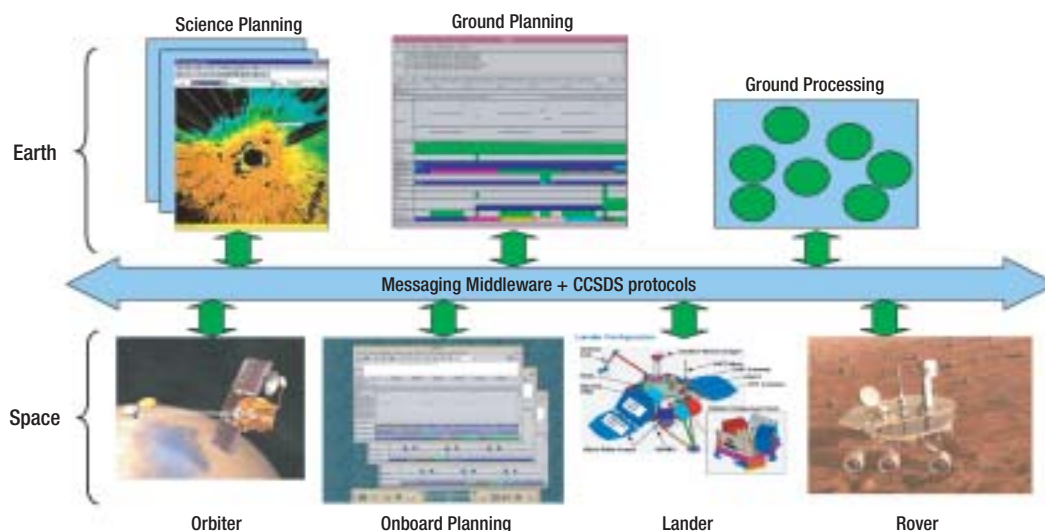


Figure 2.  
Middleware-enabled space web

*Formation flying:* Middleware can significantly simplify the local distribution of information (e.g., location, time, and sensor data). This could be particularly necessary when spacecraft need to collaborate in real time, e.g., for coordinated science observations or formation flying.

*Advanced spacecraft computing and autonomy:* Middleware can simplify access to computing resources. A simple, low-cost node could thus perform much more complex work by leveraging off-board assets. Similarly, onboard autonomy attempts to make decisions based on available information; a space web could provide more timely and useful information in appropriate form (e.g., from a remote-sensor feeds) to support such decision-making, particularly in the case of distributed planning. From a goal-based (science or engineering) perspective, space middleware could support distribution and negotiation of lower-level activities (elaborated from high-level goals) among cooperating (communicating) craft.

*Active and passive remote sensors:* A sensor web could form a simple space information web. Data collection, distribution, and processing could be simplified for all types of sensor information at various levels (from raw to interpreted), thus effectively leveraging the potential contribution of every sensor. For example, a passive sensor could simply publish regular measurements for consumption and action by more complex, active nodes.

*Agent communication, fault recovery:* Agents process known types of information by applying rules to create actionable outputs. A simple example is an onboard agent reporting vehicle health or sensor status to external recipients. More complex agents could then provide processed information, e.g., generating a science alert based on receiving and correlating distributed sensor data.

A space web could thus increase science quality and reduce operations cost, as well as making individual missions simpler and more robust, thereby reducing risk. As such capabilities evolve, a science researcher could ask progressively higher-level questions and specify rules, which could be successively

broken down into many (automated) tasks involving data acquisition, processing, and analysis. Space and ground components are both needed to support the architecture, but would be tailored for each environment (space versus ground), and built upon common standards in each domain (e.g., CCSDS versus Internet protocols).

### **Approach**

In order to support this integrated vision, we believe it is necessary to consider interoperability at three levels: application, middleware, and communications, as shown on the left side of Figure 3. At the highest level, applications (software modules, agents, and mission components) need to share and process data and information seamlessly even when the other layers have been implemented (and perhaps designed) independently. Different layers thus represent different levels of conceptual or physical interoperability. The objective of our work is thus to make an intellectual connection between the service-based architecture evolving in today's business Internet, and the future interplanetary network architecture mentioned above. Our first goal is to define and explore the capabilities of space-based middleware to provide future missions with such new capabilities. We need to show flexibility for different standard communication protocols (such as CCSDS Proximity-1) to plug into the lowest middleware layers; above this level, we need to define capabilities somewhat independently of the protocols.

We have identified several such capabilities that could be provided by middleware in the space domain. These include science capabilities (such as sensor information processing and management), operations capabilities (such as status monitoring and automation), and management capabilities (such as service installation, monitoring, and update). These capabilities may be viewed as distributed applications that can be built using components (such as data storage, data query, event services, and message delivery) within an integrating service architecture. Figure 3 shows some example mappings between the layered view and a service view, with example benefits tagged on the right.

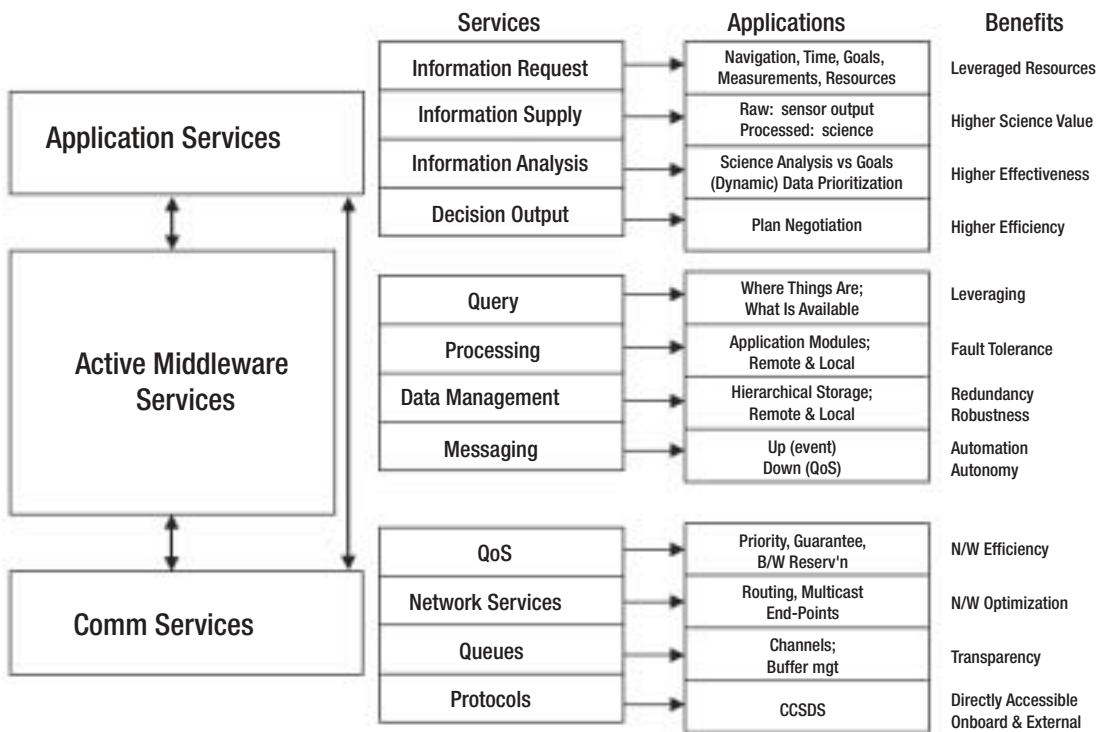


Figure 3.  
Expanded view of  
space middleware

It is also important to demonstrate that such an architecture can be incrementally developed and deployed, and that as each new component is added, significant new capabilities can be enabled when it is combined with the existing components in different ways. When we began this effort in FY02, we therefore picked the most basic level of the middleware (but also the most required) for service prototyping, namely the messaging layer. We approached this by leveraging an existing object-based MOM infrastructure (SharedNet), developed by JPL for the US Marine Corps to transfer information along the command chain down to Marines in the field. A key requirement was efficiency in both what and how information is transferred, and also the ability to deal with intermittent and low-bandwidth connections (e.g., hand-held radios). These requirements show striking applicability to the space domain. We therefore utilized some IND technology funds to apply this MOM technology to a proof of concept for the proposed space service architecture. At the application level, we chose a scenario involving simulated three-way communication between two rovers (MER-A and MER-B) and an orbiter (Odyssey). The scenario's goal was to show how critical information

could be turned around more rapidly and automatically between one of the rovers and Earth by flexible relay and replanning. The scenario had been constructed previously in FY01 as a demonstration of distributed planning, but without a communications mechanism suitable for deep space. Our prototype attempted to show that, with some modification of the application, we could provide significant additional capability (including robustness) using the MOM approach.

Because SharedNet's data object model is known to all parties, it can significantly simplify the creation of new application protocols and reduce the amount of data required for transfer. For this example, we created a new "Activity Type" in the object model, and used this in the plan negotiation, transferring only attributes and not the entire activity objects. We therefore used the existing middleware to encode, transfer, and decode the parameters, since this was part of the MOM. By extension, other kinds of information could be transported efficiently and simply, merely by extending the object model to include the desired objects, e.g., instruments, resources, or entire spacecraft. Such unification of approach in describing such objects could

significantly simplify building onboard applications as well as providing immediate access to the middleware features (such as reliable transport, remote query, event processing, etc.). Our prototype activity continues at low level (under IND technology funding), and this year is focused on how higher-level applications can be layered on top of the robust messaging middleware. We have therefore chosen an onboard science application, again developed by others, and hope to show the increasing range of potential capability via incremental evolution of the middleware.

### **Conclusions**

Space-based middleware can help shift focus away from the details of point-to-point remote communication and towards a high-level service architecture with increased capability for automation and cooperation among space assets. A first step is to define high-level data objects and a mechanism to allow efficient exchange between producers and consumers interested in particular attributes of such objects. This step helps on-board applications to be insulated from inessential details (including the vagaries of the space communication). We believe many of these details are best handled by software developed once (at the shared service layer), rather than inside every individual application.

We distinguish the suggested space middleware service architecture from the

(required) underlying communication protocols. Of course, such middleware cannot be deployed in space without careful attention to its particular constraints (e.g., intermittent connectivity, limited resources such as bandwidth, power, etc.). Moreover, reliability and availability become paramount for services in the space domain, and need to be addressed much more carefully than is typical for Internet-based services. For example, automated transparent service redundancy would be an important goal.

We also need to define interfaces to appropriate higher-level peer information services (as in the middle column of Figure 3), and to design these services to be layered appropriately despite the highly resource-constrained environment. Our suggested approach is to follow the incremental development of terrestrial web services, which are based on encapsulated components communicating via Internet protocols. As observed with the terrestrial Internet, functionality and benefits would increase as more services are deployed and more resources (spacecraft) cooperate.

This work was performed at the Jet Propulsion Laboratory of the California Institute of Technology under a contract with NASA. Original contributions of Anthony Barrett, Thom McVittie, and Brad Clement are acknowledged, as is the pioneering work by Kevin Delin in sensor webs.



# UAV-to-Ground Optical Communications Transceiver

## Introduction

The Multi Agency Program Office at JPL, with funding from the Missile Defense Agency (MDA) and Space Missile Defense Command (SMDC) initiated the Unmanned Aerial Vehicle (UAV)-to-Ground Laser Communications Demonstration project. The objective is to demonstrate bidirectional laser communications from an airborne UAV to a fixed ground station in daytime and nighttime conditions. The planned demonstration will emphasize a high-rate (0.6–2.5-gigabit-per-second [Gbps]) downlink from an airborne UAV at cruise altitudes to a ground receiving station, with a simultaneous moderate-rate (~10 megabits-per-second [Mbps]) uplink, implemented by modulating a laser beacon transmitted from the ground station. The asymmetric air-to-ground data exchange is for the purposes of reducing complexity and cost of the demonstration and is not a limitation of laser communications systems.

State-of-the-art UAVs such as the Predator and Global Hawk have the capability of communicating with satellites at 3- and 50-Mbps rates. In order to achieve the rates, the Global Hawk, for example, is equipped with a 1.2-meter (m) (48-inch)-diameter zenith-pointing K-band antenna. The relatively large, gimbaled antenna compromises maneuverability of the aircraft, aside from using up potential payload space. In comparison, optical systems 10–30 cm in diameter will be capable of providing at least 2–10-Gbps data rates on a UAV satellite communications link.

Demonstrations of higher-bandwidth communications from UAVs are driven by the Department of Defense (DoD) and National Reconnaissance Office (NRO), because they need rapid transfer of huge data volumes from remote locations to command centers.

Future battleground theater operations and reconnaissance will increasingly rely upon such capability. The sensors used for acquiring such high volumes of data are potentially hyperspectral imagery, synthetic aperture radar (SAR), and high-definition television (HDTV) cameras. Immense benefit for NASA's Earth science applications can result from the availability of optical communications technology as well, especially for disaster monitoring and performing high-resolution scientific imagery for mapping and monitoring the Earth.

As an example, the Airborne Synthetic Aperture Radar (AIRSAR) instrument operated by JPL acquires a 15-kilometer (km)-wide swath of data over a 10-minute duration. This translates to a scan length of 123 km on the ground, equivalent to the distance traversed by the DC-8 aircraft that transports the AIRSAR instrument. The AIRSAR raw data acquisition rate of 80 megabytes per second (MBps) results in a 384-gigabit image. With some overhead this data could be transferred over an optical link (1–10 Gbps) in 1–10 minutes, or times no greater than that required for acquiring the image. Optical links are a potential means of streaming and routing the data in near real time to scientists or other customers. Indeed, recent optical communications demonstrations from geostationary orbit underscore the viability of a distributed network of air, space, and ground assets configured as a high-bandwidth optical network. NASA and the DoD are including the development and deployment of the optical infrastructure in their future plans.

This article emphasizes the optical communications terminal (OCT)

*Abhijit Biswas  
and  
Keith E. Wilson*

development key to enabling the demonstration objectives. In order to better understand the OCT design drivers, a brief description of the UAV platform and operations scenario is given next, followed by a description of the current design

### Description of UAV-to-ground demonstration

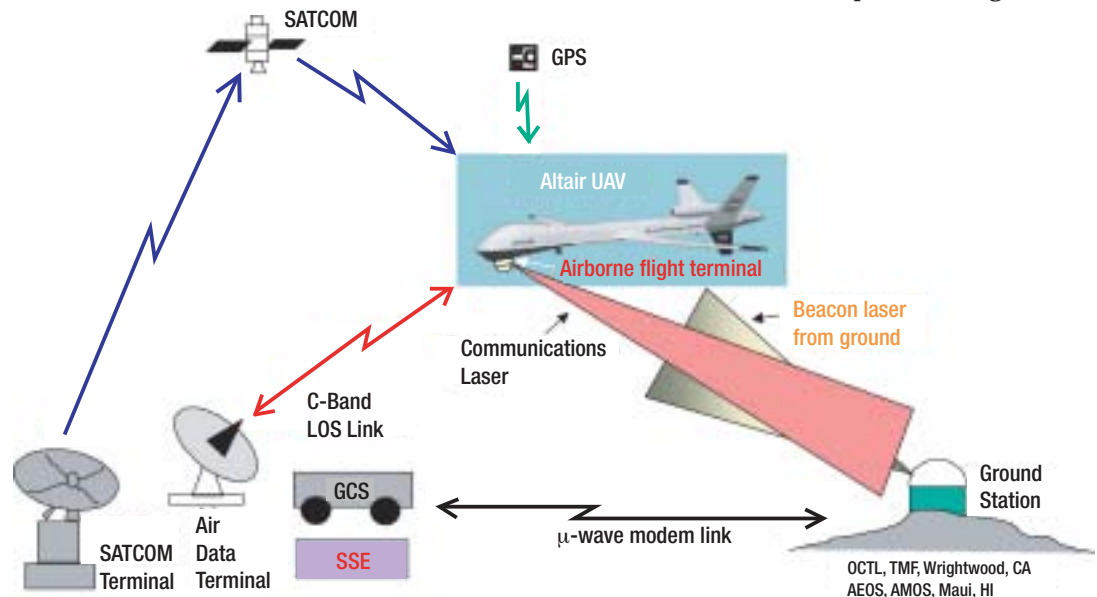
The Altair UAV platform currently selected for the demonstration is manufactured and operated by General Atomics, Aeronautics Systems, Inc. of Rancho Bernardo, California. The Altair is a version of the Predator-B. It has a larger wingspan and cruises at altitudes upwards of 15.8–16.7-km (52–55 kilofeet [kft]) for very long durations (up to 32 hours with full payload of 660 lb and maximum fuel). Currently, the Altair aircraft have an interface for a nadir-mounted turret assembly that houses an imaging sensor. A 0.36-m (14-inch) turret assembly manufactured by Wescam, Inc. is most commonly flown, though larger turret assemblies can also be accommodated. For our demonstration we are pursuing an approach that will involve retrofitting the JPL-developed OCT to the 0.36-m Wescam turret assembly. The Altair can be flown using line-of-sight C-band links or over the horizon Ku-band Satcom links. Figure 1 shows a schematic view of the lasercom demonstration that, according to current schedule, should occur in the 2005–06 time frame, provided funding is available.

The ground receiving stations for the demonstration will utilize JPL's Optical Communications Telescope Laboratory (OCTL), and the Air Force research Laboratory (AFRL) telescope at Mt. Haleakala, Maui, Hawaii. Appropriate instrumentation developed by the project will be retrofitted to these ground telescopes.

The nominal operation scenario will involve the UAV executing a predetermined track around the ground station. The ground station will acquire and track the aircraft, while illuminating it with a beacon laser beam to initiate the optical link. Aircraft global positioning system (GPS) coordinates will be relayed to the ground station over a separate radio frequency (RF) communications link to aid the initial acquisition of the aircraft by ground. The optical terminal aboard the UAV will be preprogrammed to point towards the ground station based upon knowledge of the updated aircraft GPS and inertial navigation system (INS) inputs and fixed ground station coordinates. After a search-scan, the terminal will, acquire the beacon and initiate tracking and simultaneous pointing of the downlink laser beam, modulated with high-rate data. The described scenario will have to compensate for disturbances caused by aircraft platform attitude fluctuations and vibrations, as well as effects due to atmospheric turbulence upon the propagating laser beams.

Allied issues related to interfacing a lasercom terminal with potential high-

Figure 1. Schematic view of the planned UAV-to-ground optical communications demonstration.



data-rate science instruments like AIRSAR and strategies for assuring quality of service for data delivered to the ground are also being addressed. In fact, as a precursor to the UAV demonstration, there are plans to fly OCT on the NASA DC-8. This will enable validation of the interface between high-data-rate science sensors and the optical communications system with end-to-end near-real-time science data being streamed to the ground. At the same time, flying on the DC-8 will serve as a risk mitigation exercise, since it will allow human-tended operation of OCT in a relatively benign environment in preparation for the autonomous scripted operation required for the UAV-to-ground demonstration.

### **Optical Communications Terminal Design Considerations**

The OCT development is being pursued so that, in addition to satisfying immediate functional and interface requirements for the UAV-to-ground optical link, scalability to longer satellite ranges is not overlooked. In other words, the OCT design architecture will be adapted in future terminal designs for communication links from UAVs to lower-Earth orbit (LEO) and geosynchronous-orbit (GEO) assets. The NASA-JPL patented laboratory prototype optical communications demonstrator (OCD) developed in 1997 is an existing example of a terminal design based upon architecture, scalable with communications range. OCD has been used for numerous laboratory experiments and two mountaintop-to-mountaintop demonstrations. OCD currently cannot support the Gbps data rates and the UAV operating environment unless major modifications are implemented. Therefore, OCT is being developed as a modified version of the existing OCD. The main modifications are an optical design that accommodates the use of high-data-rate 1550-nanometers (nm) erbium-doped fiber amplifier lasers and an expanded field of view. The latter will be compatible with the higher expected attitude variations for an airborne platform.

The OCT is an afocal telescope with a shared transmit-receive aperture. OCT will have several optical channels. 810-nm beacon

laser light received from the ground will be collimated and focused simultaneously on a high frame rate CCD tracking array and a data detector. The field of view of each of these sensors is  $\pm 5$  millirads (mrad). The single-mode fiber output of an erbium-doped amplifier is coupled to OCT. The laser transmitter can thus be located remotely from the optical head. After collimation, the 1550-nm laser beam is reflected off a fine-steering mirror (FSM) located at an aperture plane of the optical system, prior to being guided out of the telescope. This allows steering the exiting laser beam over a  $\pm 5$ -mrad angular region in the far-field of OCT. Prior to exiting the telescope system, the 1550-nm light path is coincident with the received beacon laser (810-nm) light path, though they are propagating in opposite directions. This is achieved by using a dichroic beam splitter. Through selection of optical components, subaperture or full-aperture illumination of the OCT primary mirror with the exiting 1550-nm light can be achieved. In this manner the angular beam divergence of the laser beam exiting OCT can be varied from 37–200 microradians. Note that the divergence cannot be varied in real time, but will require disassembly and switching of optical components. The FSM updates, by the acquisition tracking and pointing control subsystem, are based on maintaining a fixed offset between the received and transmitted laser beam. This is implemented by continuously monitoring the centroids of the transmitted and received laser beams on a fast-frame-rate tracking sensor operating in a multi-subwindow-framing mode. However, 1550-nm laser light is not sensed by the tracking-focal-plane array silicon sensor. Hence, a low power 980 nm laser light is multiplexed with the 1550-nm emission of the fiber amplifier laser so that a pointing reference spot is incident upon the tracking-focal-plane array when OCT is transmitting a laser.

The UAV airborne attitude variation amplitudes and rates will be relatively high compared to a stabilized space platform. The attitude rate fluctuations can be accommodated by the pointing and

tracking-control loop design, however, initial acquisition can be a problem. To overcome this limitation, a coarse acquisition camera with a  $\pm 1.5^\circ$  field of view that uses a separate aperture, co-boresighted with the main aperture of OCT will be implemented.

Figure 2 shows a block diagram and Figure 3 is an isometric view of the OCT assembly generated using a ray tracing program.

The optical head will be integrated with the 0.36-m Wescam gimbal, as mentioned before. The command and control electronics including the laser will be packaged in an electronics box. An umbilical cord comprising all the necessary signal cabling and the optical fiber from the laser

transmitter will interface the optical head with the electronics box of the OCT.

The laser power required to support the UAV-to-ground links is 50–200 milliwatts (mW), taking into account adequate margin for atmospheric attenuation and atmospheric turbulence induced irradiance fluctuations. The OCT design will accommodate transmission of 1–2 W of optical laser power at 1550 nm. Figure 4 shows a composite view of the separate components of the OCT. The total mass of the optical head with gimbal will be approximately 40 kilograms (kg), with an additional 25 kg allocation for the electronics box, and the power consumption will be approximately 100 W.

Figure 2. Block diagram of the OCT optical head design.

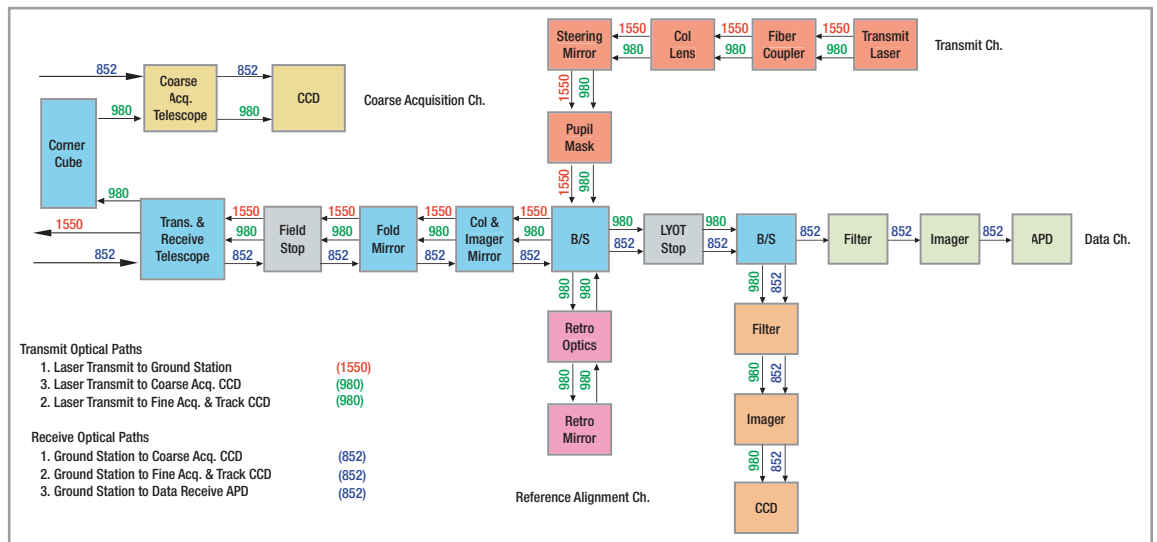
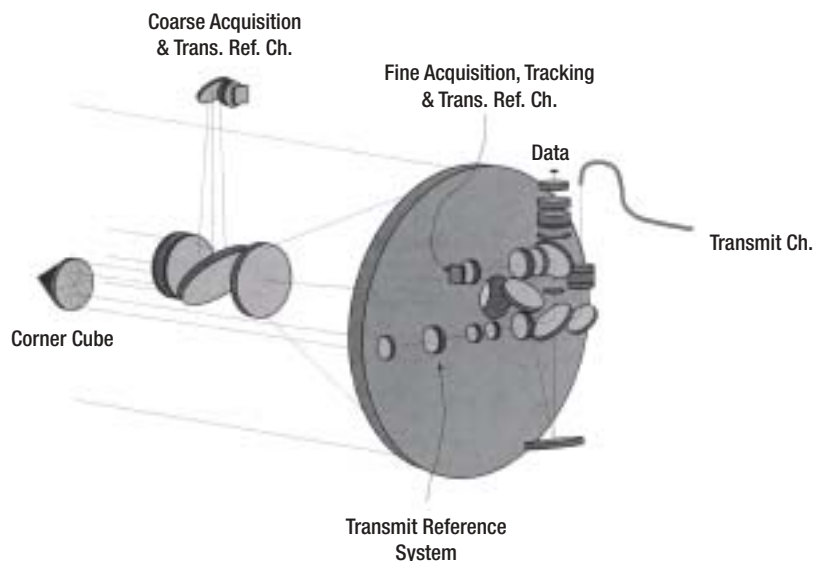


Figure 3. An isometric view of the optical assembly design generated using Code V ray tracing software.



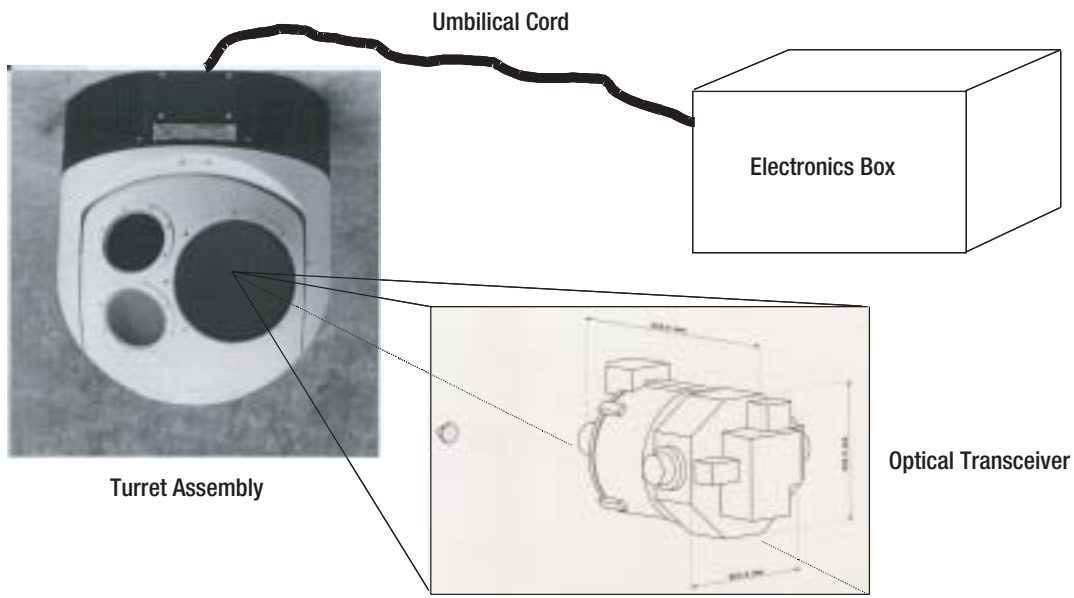


Figure 4.  
A composite view  
of the elements of  
OCT.

**Conclusion**

A successful completion of the stated objective, we believe, will serve as a key milestone for equipping UAVs with high-bandwidth, low mass, agile communications

systems. This in turn will enable UAVs to serve as a node in a high-bandwidth network that can include satellite, ground, and other airborne assets.



# The Large Millimeter Telescope

*Alfonso Feria*

## Introduction

The Large Millimeter Telescope (LMT) project is a joint effort between the University of Massachusetts (UMass) at Amherst and the Instituto Nacional de Astrofísica Óptica y Electrónica (INAOE) in Mexico. The LMT will provide a 50-meter (m)-diameter, millimeter-wave telescope designed for principal operation at frequencies between 100 and 300 gigahertz (GHz) (see Figure 1). To meet its goal of making the highest-sensitivity measurements ever achieved at these wavelengths, the LMT primary reflector will enable it to “see” light emanating from the first visible structures in the universe. The telescope is being built atop Sierra Negra, a volcanic peak in the state of Puebla, Mexico. Site construction is underway, along with fabrication of most

of the major antenna parts, with telescope construction expected to be complete by the end of 2004. The Jet Propulsion Laboratory, through funding from the Department of Defense Advanced Research Projects Agency (DARPA), is providing engineering support during the design, fabrication, and construction phases of the telescope project.

## Antenna Location

The Sierra Negra site (Figure 2) was selected in 1997 following radiometric site tests at a number of potential mountaintop sites in Mexico. The 19° latitude was a significant factor in the site selection: the LMT’s coverage of the southern sky will be very good, with the galactic center culminating at an elevation of about 45°. The site is at a very high elevation (4,600

Figure 1.  
LMT antenna  
main subsystems.

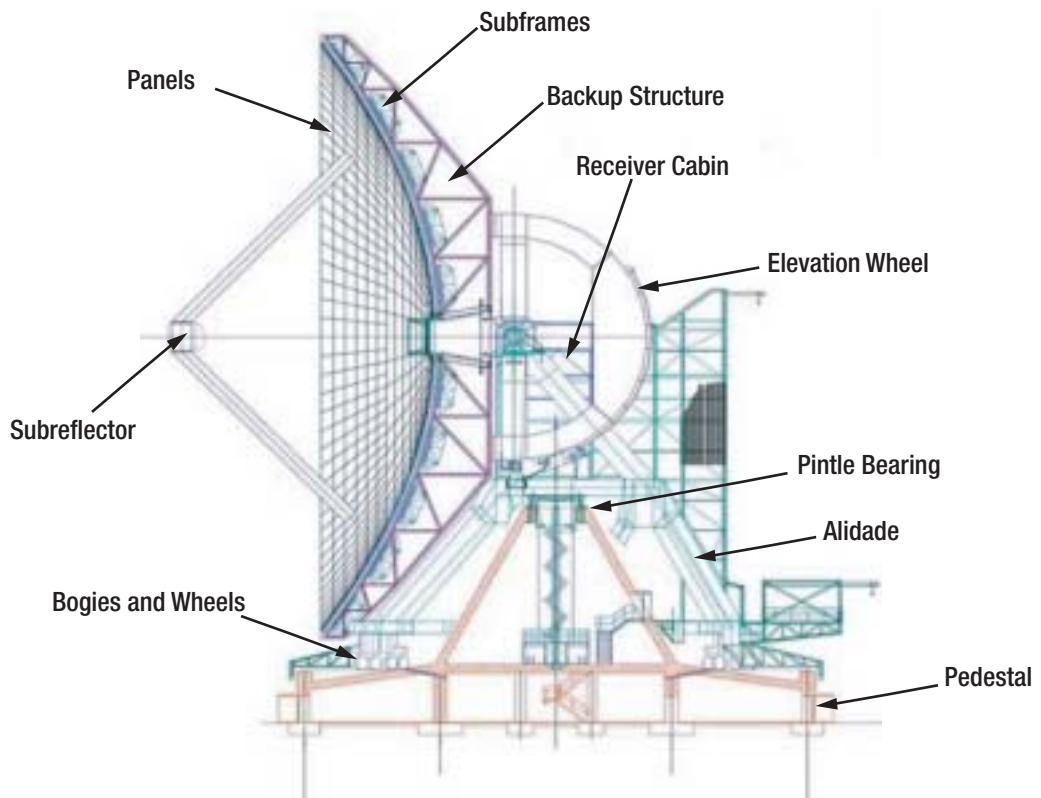




Figure 2.  
Telescope  
construction on top  
of Sierra Negra.

meters [15,000 ft] above sea level), which was found to be necessary in order to achieve the best opacities. The atmospheric opacity, as measured by a 225-GHz tipping radiometer, is low for most of the year. The summer months are relatively humid and cloudy so that the best high-frequency observing conditions occur during the winter months.

The meteorological conditions at the site are relatively mild for such a high altitude. For antenna performance, the most critical factor is the wind speed, since the wind distorts the surface of the dish and affects the antenna pointing. The median wind speed is only 6 meters per second (m/s); the telescope has been designed with the goal of meeting its specifications in a wind of 10 m/s. Snowfall is generally light during the year, and the diurnal temperature cycle is typically only 5°C.

Even though the site conditions are relatively mild, it must be realized that operation at the site will not be a trivial matter. First, the high altitude is a significant problem, which will be addressed with oxygen enrichment of key rooms at the telescope site and development of a good remote-observing capability that will enable visitors to operate the telescope from a more favorable altitude. Lightning has been a major problem for the

site as well, and it has made maintenance of site test equipment difficult. Improved grounding of test equipment has made for more reliable operation, and a final grounding design for the telescope has been completed. Finally, some extreme weather conditions, such as brief, intense storms, also exist. Care must be taken to provide for shelter at the site, in case workers become stranded by bad weather and for protection of the structure under heavy weather conditions.

Access to Sierra Negra is very good. Most of the travel distance from Mexico City (approx. 250 kilometers [km]) and Puebla (approx. 100 km) is via one of the major east-west divided highways in Mexico. A temporary road has been constructed to the top of the mountain for access during construction, and an electrical power line has been installed. Improvements to the access road are planned for the transportation of some of the larger telescope pieces. A new permanent road, for site access in the long term, is under construction by the state government of Puebla. The total travel time from INAOE (located west of the City of Puebla) to the mountaintop is about two hours.

### Telescope Description

The antenna construction project is now advancing rapidly, with contractors having been selected for most of the key telescope subsystems. Figure 1 summarizes the major telescope subsystems.

The telescope is supported by a concrete cone and a concrete pedestal, including seventeen concrete piers, drilled to a depth of 18 m to ensure attainment of the telescope's stringent pointing requirements. It has an azimuth mount consisting of a pintle bearing, mounted on top of the cone, and four bogies with four wheels each, rolling on an all-welded, single-piece steel track. The steel alidade structure supports the tipping structure (see Figure 3) and the receiver cabin where the telescope instruments will reside.

Stainless steel subframes support the telescope's surface panels and are attached to the steel backup structure by actuators (see Figure 4). These actuators will be used to correct the surface due to gravity deformations as the telescope moves in elevation. The panels and the subreflector are being manufactured of carbon fiber reinforced polymer (CFRP) material using aluminum skin as the reflective surface. The LMT requires a total of 180 panels

to complete the 50-m-diameter primary reflector surface. Since the antenna surface panels are considered the limiting factor for future surface performance enhancements, the panel surface errors are being pushed as low as is economically possible (to 20 microns root mean square [rms]). The LMT subreflector is a high-quality mirror (12 microns rms) with a diameter of approximately 2.6 m.

This has become a highly international project, with design carried out by a German company; fabrication of the concrete pedestal, structure, track, subframes, panels, and subreflector by Mexican companies; some mechanical components by Italian companies; engineering design and analysis by U.S. consultants; and so forth.

### Scientific Instruments

With nearly 2000 m<sup>2</sup> of collecting area and a surface accuracy better than that of the Spanish Institute for Millimeter Radioastronomy (IRAM) 30-m telescope, the LMT's sensitivity will exceed that of its nearest competitors by a wide margin. This basic sensitivity is enhanced, for continuum observations, by the single dish's ability to make use of incoherent detectors. Moreover, as a completely filled aperture, the LMT

Figure 3.  
Backup structure  
shop preassembly.



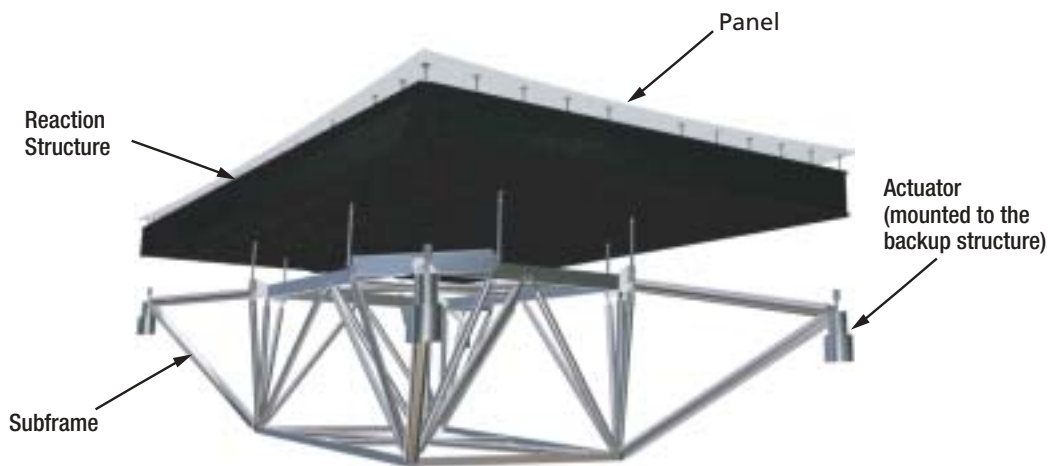


Figure 4.  
Panel assembly.

will have the optimum sensitivity to low surface brightness emissions at an angular resolution (6–12 arcsec), which is comparable to maps presently made with interferometric arrays. As such, the LMT will take a valuable place in the world's present complement of millimeter-wave facilities.

The binational LMT Science Team has selected an initial set of instrumentation that emphasizes the special capabilities of the large single dish, as well as the practicalities of beginning to commission and operate the telescope. Some of the instrumentation is well advanced, and other instruments will be built in the next few years.

Some of the instrumentation being considered for the LMT includes:

- Sequoia, a focal plane array for observations in the 3-millimeter band that will include galactic and planetary science, with focal plane arrays, kinematic studies of star forming regions, and CO mapping of galaxies
- Correlators, including spectrometers for all LMT receivers
- Bolocam, a focal plane array for continuum observations for studies of the distribution of thermal dust in the galaxy, extragalactic studies of galaxy counts and distributions, the Sunyaev-Zel'dovich effect, observing strategies, and telescope modes
- Redshift Machine, a new kind of instrument designed to search for lines in the redshifted CO ladder

- Commissioning Instruments for the characterization of LMT performance and initial science: both 3-mm- and 1.3-mm-band receivers are being considered
- Support Instrumentation, including a wave-front sensor to measure the tilt of the incoming wave front so that atmosphere-induced pointing errors may be removed and a holography receiver may make measurements of the antenna surface at the time of its initial setting.

### Conclusions

The LMT will be a significant step forward in antenna design since, in order to reach its pointing and surface accuracy specifications, it must outperform every other telescope in its frequency range. The largest existing telescope with surface error superior to the LMT is the 15-m James Clerk Maxwell Telescope (JCMT) in Hawaii, and there is no telescope of any size that reaches the LMT pointing requirements. The LMT is expected to be in operation in 2005, and further improvements in operational requirements are expected to continue.

For further information contact Alfonso Fera or visit the LMT Web site at <http://www.lmtgm.org/>



# MASERs, Black Holes, and the Age of the Universe

*Tom Kuiper  
and Lincoln  
Greenhill*

Figure 1.  
NGC4258  
(M106) lies in  
the constellation  
Canes Venatici  
( $12^h 19.0 + 47^\circ 18'$ ).  
It contains the most  
spectacular water  
MASERs circling a  
black hole. (With  
permission of  
Christian Deforet:  
Centurion 18".)

During the southern winter of 2002, the Canberra 70-meter (m) antenna was used to discover water-rich clouds circling at high speed around the centers of galactic nuclei and emitting intense microwave beams. The observations significantly increased the number of galactic nuclei known to contain these water MASERs.<sup>1</sup> To enable this search, the Smithsonian Astrophysical Observatory (SAO) acquired a special-purpose spectrometer at a cost of \$75,000. The SAO scientists have also spent a total of about ten months over the last two years at the overseas Deep Space Network (DSN) complexes working with local scientists.<sup>2</sup> What motivates this financial investment and the efforts of a large international team of astronomers?

## Objectives

NGC4258 (Figure 1) appears at first glance to be a galaxy not very different from our own. It has the characteristic spiral pattern and a central bulge common to many such galaxies. It is about  $18' \times 8'$  in size or  $110 \times 50$  kiloparsecs (kpc).<sup>3</sup> However, it is one of a minority that contains jets of material flung out of the nucleus by some central source of energy. Figure 2 presents a montage of one of the most famous galaxies among optical and radio observers, M87, showing jet-like emission over a huge range of size scales.

<sup>1</sup>MASER: microwave amplification by stimulated emission of radiation; also used to describe an intense radio source radiating by this mechanism.

<sup>2</sup>Jet Propulsion Laboratory, Astrophysics and Space Physics Section and Interplanetary Network Directorate (IND) Science Office

<sup>3</sup>A parsec (pc) is 3.26 light years. The Sun is about 8.5 kpc from the center of our galaxy.



NGC4258 is also one of a handful of this minority that also exhibits intense MASER emission from hot water vapor clouds near its nucleus.

The large Doppler velocities of some of these MASERs as they approach and recede from us show that they orbit very close to a large mass. MASERs in smaller orbits have higher orbital speeds, as we expect from Newton's Law of Gravitation, and therefore higher Doppler shifts. (Viewed from another star, our solar system would appear to behave similarly but on a much smaller scale; Jupiter circles the Sun in about 12 years while Mercury completes a circuit in only 88 days.)

Figure 3 shows how gas circling a central object is blue-shifted (Doppler-shifted to higher frequency) where it approaches the telescope (lower wave) and red-shifted (Doppler-shifted to lower frequency) where it recedes from the telescope (upper wave). Figure 4 shows the Doppler velocities of water MASERs in galaxy ESO269-G012, one of those discovered in Canberra in 2002, and quite similar to NGC4258. Here the rotation speed is about 600 kilometers (km) per second!

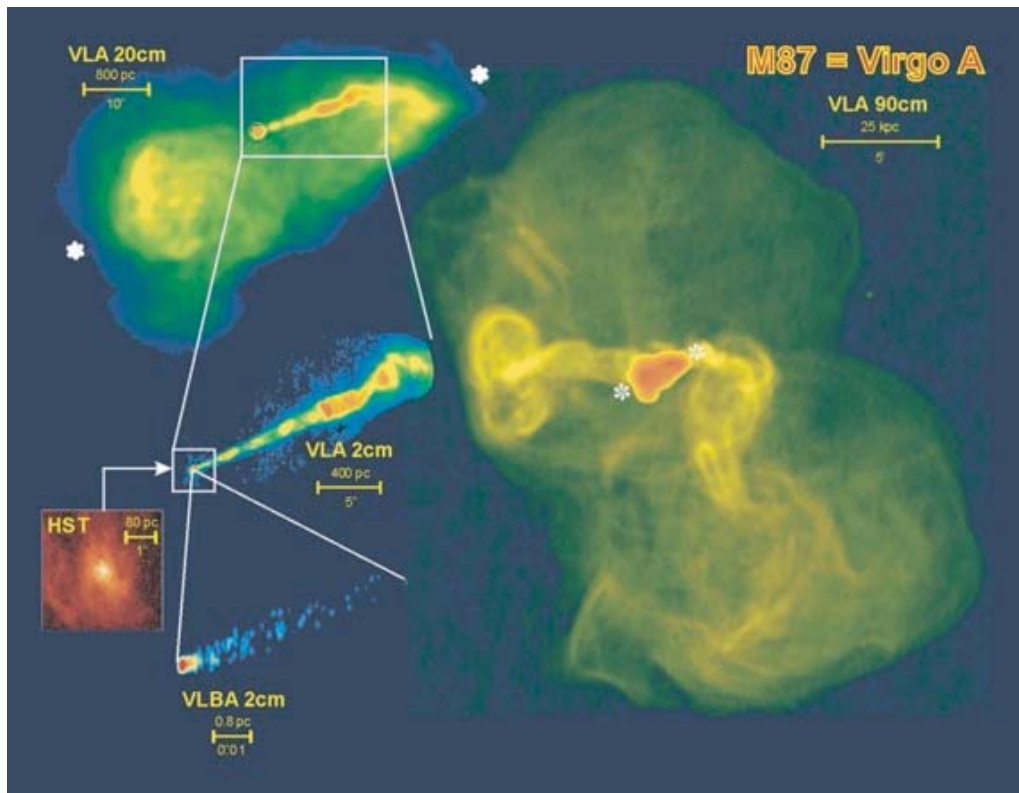


Figure 2. This montage of M87 was obtained from the National Radio Astronomy Observatory (NRAO) Image Gallery at [www.nrao.edu/imagegallery](http://www.nrao.edu/imagegallery) and used with permission from NRAO; Associated Universities, Inc.; and the National Science Foundation.

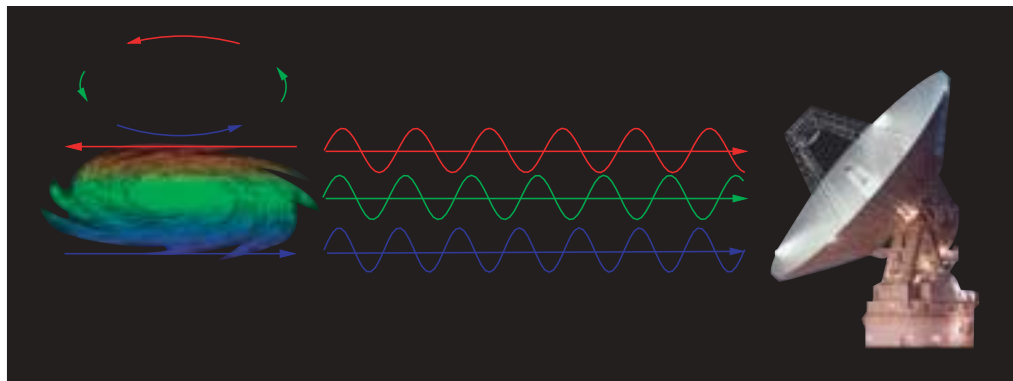


Figure 3. High- and low-velocity MASER features are produced by the Doppler shift of gas circling at high speed around the nucleus of a galaxy.

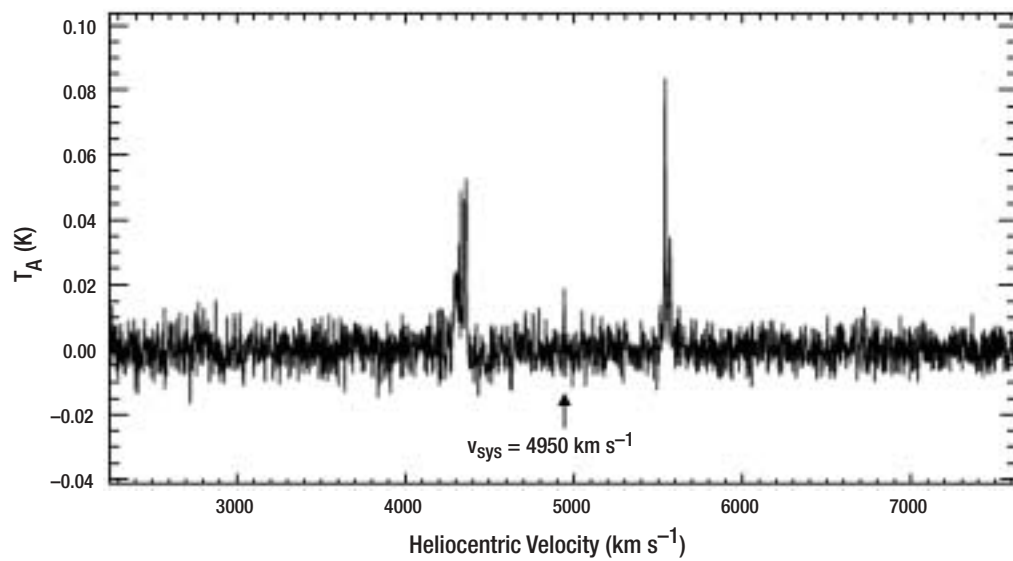


Figure 4. The spectrum of water emission from ESO269-G012 shows there is gas moving at +600 and -600  $\text{km/s}$  around the center of the galaxy. Overall the galaxy is moving away from us at about 5000  $\text{km/s}$  as the universe expands.

What makes NGC4258 and similar galaxies so interesting is that through study of the orbiting MASERs, astronomers can measure accurate distances merely from simple geometry. Not all the gas is red-shifted and blue-shifted. In a circular orbit, some gas moves across our line of sight to the center of the orbit. It has no Doppler shift, but it does have what is called a proper motion: an angular velocity across the sky. For NGC4258, an international team of scientists has used very-long-baseline interferometry (VLBI) to measure this proper motion, with stunning consequences. One set of MASERs provides the orbital velocity in kilometers per second (the Doppler shift) and the other in arcseconds per year (the proper motion). The ratio of the two is distance, which is unambiguously 7.2 million parsecs (Mpc), for NGC4258 with an accuracy of 4%.

Astronomical distances are usually estimated from the apparent brightness of objects whose actual luminosity is known. These objects (for example, Cepheid variable stars and certain kinds of supernovae) are called "standard candles." However, assumptions and corrections must be made to compensate for differences among candles from galaxy to galaxy, and so resulting distance measurements are susceptible to systematic uncertainties that are sometimes difficult to characterize. This weakness is what makes MASER distances, such as the one to NGC4258, so immensely valuable.

A long-term goal of the SAO project is to find more galaxies the distance of which can be determined geometrically with water MASERs. Such distance measurements are accurate and unambiguous. They are independent of systematic uncertainties common to analyses of standard candles. This would permit the standard candles and all existing distances to be calibrated more securely. All this should lead to a more reliable value of the Hubble constant, cosmic acceleration, and the time since the "Big Bang."

An additional goal is to detect and measure black hole masses with high accuracy. For example, with the distance to NGC4258 established, the angular

separation of the blue- and red-shifted MASERs gives the radius of the ring of gas. With the radius and the rotational velocity of the ring, Newton's Law provides the mass interior to the ring: 39 million solar masses within a radius of one third of a light-year. Only a black hole can pack that much mass into so small a region, and this one has been weighed with an accuracy of only 4.

The study of MASERs makes it possible to map the shapes of accretion disks less than a light-year from the supermassive black holes. This has provided the first conclusive evidence that these disks are warped. Follow-up investigations have suggested that it is possible for warped disks to channel radiation, winds, and outflows driven by black holes, thereby determining the extended appearance of galactic nuclei. Radioastronomical techniques are currently the only means by which to study these heavily obscured regions in the hearts of galaxies. Gas and dust along the line of sight block optical, infrared, and in extreme cases even X-ray light. Nonradio telescopes as well are limited to angular resolutions at least two orders of magnitude worse than radio interferometers.

To date, about ten MASERs with high-velocity emission are known to exist. With so much to gain from the study of water MASERs around galactic nuclei, the motivation to expand this class of objects beyond NGC4258 is high.

### **Why the DSN?**

Although the DSN complexes are tracking stations, they are also remarkably capable radio observatories. At 22 gigahertz (GHz), the 70-m antenna at Canberra is the most sensitive antenna in the southern hemisphere by at least a factor of ten.

Another feature is a research and development (R&D) environment into which investigators can integrate their own equipment and which can be adapted to their requirements. The hardware and software for radioastronomy in the DSN was designed (and is still evolving) with this flexibility in mind.

In spite of the fact that the DSN is oversubscribed, it is still able to provide substantial amounts of antenna time to

selected radioastronomy projects. This is because spacecraft have certain view periods at each antenna, and there are times when no spacecraft is visible, at least none that need the power of a 70-m antenna. This makes the DSN a national resource for projects that need large amounts of antenna time and can accept it sprinkled around the schedule over years.

Between May 2001 and October 2002, the project has used about 470 hrs of 70-m time for observing and calibration. (About another 100–150 hrs have been spent on engineering issues which were identified by this project but which needed to be resolved for all users.) Such a large investment of time is necessary since it takes about one and a half hours per galaxy to reach the necessary sensitivity level, and the detection rate is about 4%.

### **The Search**

The search for new MASER sources is being conducted by the Smithsonian Astrophysical Maser Black Hole All-sky (SAMBA) Survey program (the Web site for which is [cfa-www.harvard.edu/samba/](http://cfa-www.harvard.edu/samba/)).

The project is led by Lincoln Greenhill of SAO. Other team members at SAO are Paul Kondratko, a Harvard graduate student who is basing his Ph.D. thesis on this work, and Jim Moran. The Australian observing team consists of Jim Lovell and Dave Jauncey of the Australia Telescope National Facility (ATNF). The Spanish observing team is led by Jose Francisco Gómez of the Laboratorio de Astrofísica Espacial y Física Fundamental (LAEFF) assisted by graduate students E. Jimenez Bailón and Itziar de Gregorio-Monsalvo. The IND Science Office support astronomer is Tom Kuiper.<sup>4</sup> The project has educational significance because it provides three graduate students hands-on experience with observing hardware and software and issues of calibration. In contrast, most students today use national or quasi-

national observatories where the equipment, software, and calibrations are maintained by the staff and which may even provide the data without involving the observers in the data acquisition.

The spectrometer was built by Spaceborne, Inc., in La Cañada, California, based on a design originally developed for a JPL millimeter-wavelength astronomy project. It is a 2-bit (4-level) digital autocorrelator based on very-large-scale-integration (VLSI) chips with 128 channels each, developed by Constantin Timoc, president of Spaceborne. The SAO correlator has 4096 channels composed of four correlator boards with eight chips each. The data are sampled at an 800-megahertz (MHz) rate, providing a 400-MHz bandwidth. (The upper bandwidth is primarily limited by heat dissipation. The JPL correlator can operate with 500 MHz bandwidth, but has only one 8-chip board in the same size chassis.)

The project is currently in its fourth season. The southern summer of 2001 was devoted to a host of engineering and calibration issues related to (1) high-frequency antenna and receiver performance, (2) refitting of the signal path for broadband data acquisition, and (3) software development. To enable these difficult observations, the characteristics of all the components in the signal path were painstakingly measured. One finding was that the tunable radio frequency (RF) filters used to define a broad RF bandpass before the downconverter are not stable enough for long integrations. Also, the R&D downconverters on DSS-43 did not have enough dynamic range. In addition, substantial reflections were found at various connectors on the intermediate frequency (IF) transmission lines from the receiver to the control room. These defects had not affected the type of observations made since the receivers were changed in the mid '90s but now had to be corrected. Some problems were solved, but others required that key components be replaced. These could not be obtained in time so no useful data were obtained.

---

<sup>4</sup>The project has received exceptional support from the overseas complexes, but special mention must be made of Graham Baines and Cristina Miro. Manuel Franco provides engineering support at JPL.

Prior to the first northern winter (2001–2002), fixed bandpass filters were acquired and the software neared maturity. The DSS-63 downconverters are of a newer type and were not a problem. Very quickly, an exceptional system temperature of about 45 K was obtained. The main issues tackled before astronomical observations could begin were antenna pointing and calibration of the spectra. This required about two months. One of the findings was that there is more radio frequency interference (RFI) near 22 GHz than is seen with DSS-43, requiring more care in data analysis. The remaining two months of the winter were used to observe about 40 galaxies, but no new sources were detected.

For the southern summer of 2002, one of the DSS-14 downconverters was sent to DSS-43 to solve the dynamic range problem. A system temperature of about 45 K was established. An RF switch matrix originally intended to direct signal from multiple front-ends to the downconverters was modified to provide remote selection of RF bandpass filters. Except for an emergency repair to the spectrometer, observations got underway quickly. The first new detection was made on June 1, 2002.

Observations for the second northern winter started in late December, after about three weeks of solving technical problems. About 100 sources have been observed to date.

Each season has seen correlator problems that have inspired design modification of existing and new autocorrelators. (JPL has two, as well as the original prototype. Another has recently been acquired by a Chinese radio observatory.) The digitizer board has been modified to provide a tunable internal clock source and an internal signal for self-testing and calibration in the field. Better shielding of the clock transmission lines suppressed artifacts in the data. Finally, the structure has been strengthened to resist shipping damage better and to improve overall stability.

## Results

The results of the DSS-43 2002 campaign have been published in *Astrophysical Journal*

*Letters* (vol. 582, p. 11) on Jan. 1, 2003. Figure 5 was taken from that paper. In each panel the arrow shows the recessional velocity of the galaxy. In the case of Circinus, water MASERS had been observed previously, but the dashed lines show higher velocity ranges in which new lines were detected.

High spatial resolution observations have been conducted with the Very Large Array (VLA)<sup>5</sup>, Very Long Baseline Array (VLBA)<sup>6</sup>, and Australia Telescope Compact Array (ATCA)<sup>7</sup>. More will be made with the Australia Telescope Long Baseline Array (AT-LBA) in the coming months. These observations will be used to obtain proper motions of the MASERS and to model the accretion disks. Because some of these sources are quite weak, the 70-m antennas will play another key role by supplementing the collecting areas of VLBI arrays, mostly comprising small (less than 25-m-diameter) antennas.

## The Future

There are hundreds or thousands of galaxies that could contain supermassive black holes and sources of water MASER emission. A current survey will probably require 1000 hours. The result should be the detection of several tens of new MASER sources, which would double the number known before the SAMBA Survey began. If one in ten is as exciting as NGC4258 or ESO269-G012, then in a few years astronomers will be hard at work on efforts to measure geometric distances to about ten different galaxies that pepper the nearby universe.

Galactic nuclei harboring black holes are key targets for current and future space missions such as the Hubble Space Telescope (HST), the Next Generation Space Telescope (NGST), the Chandra X-Ray Observatory

---

<sup>5</sup>National Radio Astronomy Observatory (NRAO) Very Large Array, Socorro, New Mexico.

<sup>6</sup>NRAO Very Long Baseline Array—a VLBI array consisting of telescopes from St. Croix to Hawaii.

<sup>7</sup>Australia Telescope Compact Array, Narrabri, New South Wales, Australia.

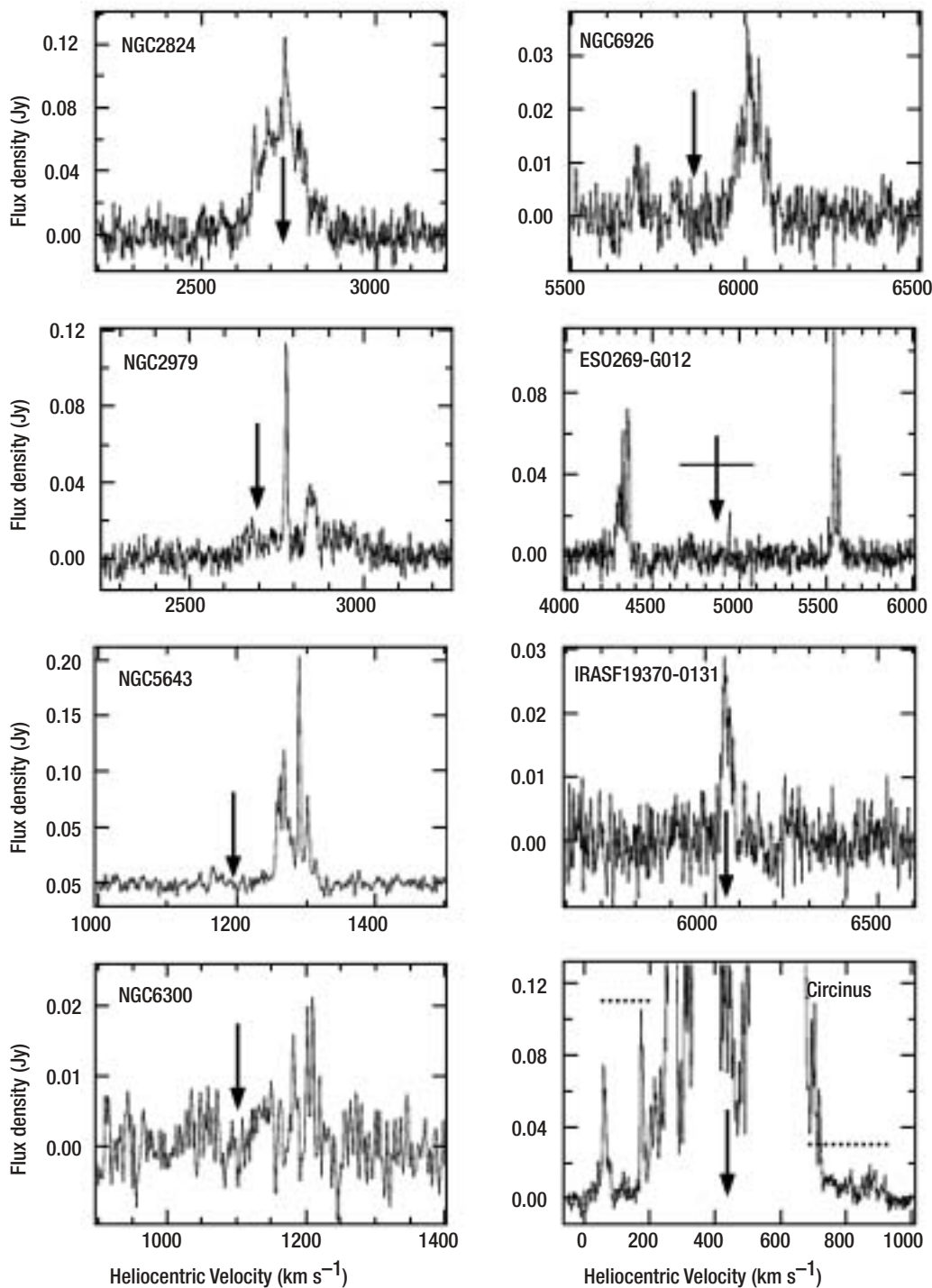


Figure 5. Spectra of the seven new high-velocity active galactic nuclei (AGN) water MASERs and the new high-velocity MASERs discovered in the Circinus Galaxy.

(CXO), and the X-Ray Multi-Mirror (XMM)-Newton. Radio observations provide complementary data not obtainable in other ways.

Since objects of this type will be prime targets for future space VLBI missions, finding them now and determining their properties lays the ground work for future missions by NASA, the European Space

Agency (ESA) and the National Space Development Agency of Japan (NASDA), and may be considered “before-the-fact,” mission-enhancing, ground-based observations.<sup>8</sup>

<sup>8</sup>MEGA (Mission Enhancing Groundbased Astronomy) is a category of DSN radio astronomy requested by space missions.



This newsletter is a publication of JPL's Interplanetary Network Directorate (IND). The IND Technology Program is managed by Jim Lesh and the Science Program by Michael J. Klein.

The IND Program Overview and related features are located at: <http://tmot.jpl.nasa.gov>. For all issues of this newsletter, click Program Overview Information and, on the resulting page, click IND News.

This publication was prepared and all work herein performed at the Jet Propulsion Laboratory, California Institute of Technology, under a contract with the National Aeronautics and Space Administration.

To add or delete your name from the IND News, contact Cruzita Abellana at 818-354-9071 or email [Cruzita.Abellana@jpl.nasa.gov](mailto:Cruzita.Abellana@jpl.nasa.gov)

*Information Systems Manager*  
*Communication Systems Manager*  
*Non-Deep Space Manager*  
*Science Manager*

*Jay Wyatt*  
*Jim Layland*  
*Charles T. Stelzried*  
*Mike Klein*

*Managing Editor*  
*Associate Editor*

*Charles T. Stelzried*  
*Christopher Weaver,*  
*Electronic Publishing Services*

*Layout and Illustration*

*Judi Dedmon,*  
*Documentation Services*  
*Jim Jackson,*  
*Electronic Publishing Services*

*Document Review*

*Kathy Lynn*



National Aeronautics and  
Space Administration

Jet Propulsion Laboratory  
California Institute of Technology  
Pasadena, California

JPL 410-066, Issue No.17 5/03

IND Technology Program Office  
Jet Propulsion Laboratory  
MS 303-407  
4800 Oak Grove Drive  
Pasadena, California 91109-8099